12-2020

High-Temperature Optoelectronic Device Characterization and Integration Towards Optical Isolation for High-Density Power Modules

Syam Madhusoodhanan
University of Arkansas, Fayetteville

High-Temperature Optoelectronic Device Characterization and Integration Towards Optical Isolation for High-Density Power Modules

A dissertation submitted in partial fulfillment
of the requirements for the degree of
Doctor of Philosophy in Engineering with a concentration in Electrical Engineering

by

Syam Madhusoodhanan
TKM College of Engineering, Kerala University
Bachelor of Technology in Electrical Engineering, 2011

December 2020
University of Arkansas

This dissertation is approved for recommendation to the Graduate Council.

Zhong Chen, Ph.D.
Dissertation Director

Shui-Qing (Fisher) Yu, Ph.D.
Committee Member

Yue Zhao, Ph.D.
Committee Member

Jia Di, Ph.D.
Committee Member

Abstract

Power modules based on wide bandgap (WBG) materials enhance reliability and considerably reduce cooling requirements that lead to a significant reduction in total system cost and weight. Although these innovative properties lead power modules to higher power density, some concerns still need to be addressed to take full advantage of WBG-based modules. For example, the use of bulky transformers as a galvanic isolation system to float the high voltage gate driver limits further size reduction of the high-temperature power modules2. Bulky transformers can be replaced by integrating high-temperature optocouplers to scale down power modules further and achieve disrupting performance in terms of thermal management, power efficiency, power density, operating environments, and reliability. However, regular semiconductor optoelectronic materials and devices have significant difficulty functioning in high-temperature environments. Modular integration of optoelectronic devices into high-temperature power modules is restricted due to the significant optical efficiency drop at elevated temperatures. The quantum efficiency and long-term reliability of optoelectronic devices decrease at elevated temperatures.

The motivation for this study is to develop optoelectronic devices, specifically optocouplers, that can be integrated into high-density power modules. A detailed study on optoelectronic devices at high temperature enables us to explore the possibility of scaling high-density power modules by integrating high-temperature optoelectronic devices into the power module. The primary goal of this study is to characterize and verify the high-temperature operation of optoelectronic devices, including light-emitting diodes and photodiodes based on WBG materials. The secondary goal is to identify and integrate optoelectronic devices to achieve galvanic isolation in high-density power modules working at elevated temperatures. As part of the

study, a high-temperature packaging, based on low temperature co-fired ceramic (LTCC), suitable to accommodate optoelectronic devices, will also be designed and developed.

Acknowledgment

I would like to thank the following people, without whom I would not have been able to complete this research, and without whom I would not have made it through my doctoral degree.

Dr. Zhong Chen, for his guidance, support, and overall insights, has made this an inspiring experience for me. He always inspired and guided me in the journey to becoming a professional researcher.

Dr. Shui-Qing (Fisher) Yu, for his expertise and guidance. Dr. Yu always amazed and encouraged me with his enthusiasm and dedication to the research.

Dr. Simon Ang, Dr. Jia Di, and Dr. Yue Zhao, for their guidance in every aspect of the research progress.

Sharon Brasko, Connie Jo Howard, Tracey E. Long, and Daniel M. Klein, for their help in administrative matters.

Abbas Sabbar, for your tremendous help and support throughout the research. It is a great pleasure working alongside you.

Dr. Sattar Al-Kabi, for helping with knowledge transfer in the initial stages of the research.

Huong Tran, for her guidance and support in developing methods for photodiode characterization.

Andrea Wallace and David Gonzalez Castillo, Pengyu Lai, for their help in LTCC packaging and characterization solutions.

Clint Hardee, for his help in assembly lab.

Hui Wang and Dan Jarard, for their numerous help in the last five years.

Alia Parveen, she always inspired me to be a better person than yesterday.

My fiancé, Sohita Ojha, for her encouragement and support.

Parents and family for their support.

The work in this dissertation was partially supported by Sandia National Laboratories, which is a multimission laboratory managed and operated by National Technology and Engineering Solutions of Sandia, LLC, a wholly-owned subsidiary of Honeywell International, Inc., for the U.S. Department of Energy's National Nuclear Security Administration under contract DE-NA0003525. SAND2019-11025 C.

Table of Contents

List of Published Papers

Chapter 3 is reproduced from the published work

S. Madhusoodhanan, A. Sabbar, S. Atcitty, R. Kaplar, A. Mantooth, S.-Q. Yu, and Z. Chen, "High-Temperature Analysis of GaN-based Blue LEDs for Future Power Electronic Applications," IEEE Journal of Emerging and Selected Topics in Power Electronics, pp. 1–1, 2019, DOI: https://doi.org/10.1109/JESTPE.2019.2945166

Chapter 4 is reproduced from the published work

S. Madhusoodhanan, A. Sabbar, S. Atcitty, R. Kaplar, A. Mantooth, S.-Q. Yu, and Z. Chen, "High-Temperature Optical Characterization of GaN-Based LEDs for Future Power Electronic Modules," physica status solidi (a), 2019, DOI: https://doi.org/10.1002/pssa.201900792

Chapter 5 is reproduced from the published work

S. Madhusoodhanan, A. Sabbar, H. Tran, B. Dong, J. Wang, A. Mantooth, S.-Q. Yu, and Z. Chen, "High-Temperature Analysis of GaN-based MQW Photodetector for Optical Galvanic Isolations in High-Density Integrated Power Modules," IEEE Journal of Emerging and Selected Topics in Power Electronics, pp. 1–1, 2020, DOI: https://doi.org/10.1109/JESTPE.2020.2974788

1. Introduction

1.1. Power Electronics and Wide Bandgap Technology

Power electronic system plays a significant role in renewable energy, energy storage, and electric or hybrid electric vehicles. As an integral part of the power electronics system, power modules provide a highly efficient form of power conversion. In the last two decades, the field of power conversion is going through a transformation where the application often demands extreme operating environments. Advancement in the field of hybrid electric vehicles, aerospace, and deep oil-gas exploration necessitates the development of power modules based on wide bandgap (WBG) devices to operate in extreme environments where the ambient temperature exceeds 200^{o}C.

Third-generation semiconductor materials such as silicon carbide (SiC) and gallium nitride (GaN) improved the operation in terms of power capability, temperature tolerance, and switching frequencies in the field of power electronics. Compared to silicon (Si) devices, WBG materials like SiC and GaN can withstand higher current densities, exhibit lower switching losses, and possess higher breakdown voltages [1],[2]. The physical properties such as lower intrinsic carrier generation at high temperature, higher breakdown voltage, and high thermal conductivity of the WBG materials enable to address the issues regarding thermal management and power density. The most used WBG materials in the field of power electronics are SiC and GaN. Table 1.1 shows a comparison of the selected material properties of WBG materials with that of Si. While GaN devices are mainly preferred for applications below 500 V, SiC is the ideal material of choice for power modules with higher voltage and current ratings. Commercially available SiC devices, rated 900 V and above, with a chip size spanning tens of millimeters, enables the development of high-density power modules with a low form factor. A small form factor power electronic system design is vital in size and weight-sensitive applications such as aeronautics, transportation, hybrid

motor drives, and space exploration. One of the driving forces behind the goal of power module miniaturization

Table 1.1. Power semiconductor material parameters at room temperature.

Material Properties		***Si***	***4H-SiC***	***GaN***
Bandgap (eV)		1.1	3.3	3.4
Mobility (cm^2/Vs)		1,400	8,000	1,200
Relative dielectric constant		11.8	9.7	9.0
Dielectric breakdown field (10^6 V/cm)		0.3	2.5	3.3
Saturation electron velocity (10^7 cm/s)		1.0	2.0	2.5
Intrinsic carrier concentration (cm^{-3})		10^{10}	10^{-7}	10^{-9}
Thermal conductivity (W/(cm K))		1.5	4.9	2.1
Defect threshold energy (eV)		9	4.9	2.1
Baliga's Figure of Merit (FOM)	Low frequency	1	340	870
	High frequency	1	50	104

is the continuous development in the system architecture and the demand from the size and weight restricted applications. Miniaturization is inevitable in the field of power electronics as much as it was in the field of integrated circuit design. The controllability of power supply, management, conversion, and conditioning is of greater importance with less expense of human intervention. WBG materials with their superior physical and chemical quality enable the researchers to explore the architectural designs to ever-smaller system footprints.

Semiconductor devices based on SiC and GaN technologies surpass the traditional Si-based devices in performance under harsh environments. The availability of SiC substrates after rigorous research facilitates the fabrication of vertical devices, which can have higher power ratings. As the cost of the device fabrication depends on the yield of the devices from each fabrication step, moving to a 150mm wafer technology from a more commonly available 100mm wafer reduced the fabrication cost exponentially. In the case of GaN devices, the non-availability of the native GaN substrate limit the vertical device design of GaN devices. However, for high-speed lateral

devices, GaN is still preferred over SiC devices due to the success in making GaN heterojunction devices with higher mobility and carrier velocity.

The device fabrication on SiC substrates initially predominated on 3C-SiC substrates. SiC can exist in different polytypes, such as 3C, 4H, and 6H. As the fabrication techniques improved, the device fabrication was mainly focused on 6H polytype substrates. In the past two decades, the majority of the SiC device fabrication is based on 4H polytype. Although SiC devices can operate in high voltage ratings, the availably of devices operating above 2 kV is still limited in the market. SiC Schottky diodes were the first group of SiC devices widely used in power electronic field due to the simplicity in the fabrication process. Researchers replaced Si Schottky diodes with SiC-based counterparts, where a higher breakdown voltage and switching speeds with minimal switching losses are necessary. These initial hybrid power module designs consist of both Si-based switching transistors and SiC-based Schottky diodes. More advanced SiC-based vertical metal–oxide–semiconductor field-effect transistor (MOSFET) devices are later introduced in the market. Although the device uses a vertical structure, the reported high voltage ratings are limited to 1.7 kV. However, these devices are far better as compared to the traditional Si devices in the critical electrical field and higher blocking voltages. Although SiC-based devices can exhibit continuous operation at high temperatures, the presence of gate oxide in the MOSFET devices limits the upper operating temperature range. To fully utilize the temperature capability of discrete SiC devices and to avoid bulky cooling systems, researched developed SiC-based bipolar junction transistors (BJTs) and junction gate field-effect transistors (JFETs), which can operate continuously at temperatures as high as 500^{o}C. Although several researchers have reported continuous operation of SiC devices with high-temperature rating in the last two decades, a fully SiC-based commercial power electronics module is still under development. The goal of full SiC-based power modules

can be achieved by the still in development SiC insulated-gate bipolar transistors (IGBTs), which possess the best features of SiC MOSFET and Si IGBT.

When it comes to GaN power devices, superior material quality is not fully utilized due to the non-availability of bulk GaN substrates. Although some researchers have demonstrated device grown on bulk GaN substrate, full commercialization is still not achieved. Due to the lack of GaN substrates, a vertical GaN-based device is not possible to be fabricated. Most of the GaN-based devices available are either high-electron-mobility transistors (HEMTs) or its derivatives. GaN-based devices are generally used in applications requiring high-speed switching and voltage ratings of 600 V and below. Although GaN is superior to SiC in terms of the critical electrical field, mobility, and saturation velocity, the lack of native GaN substrate limits its extensive use in power electronic modules.

1.2. Introduction to Optoelectronics

The information age, starting in the late 20th century, is characterized by an economy primarily based on the information technology mainly rooted by the advancement of transistors. Processing, storage, and transformation of information are prime importance in this modern era of advanced electronics. Rapid development in the field of electronics towards more complex systems to improve the performance of information handling leads scientists to find solutions based on optical means. Optoelectronics is a branch in electronics, that contributes advanced solution for information handling through optical and electronic means. Incorporating optical devices in traditional electronics tend to increase the performance of the system by achieving higher operation speeds and enhanced reliability.

The incorporation of optical devices in the information field is started when optical semiconductor devices replace old technologies such as vacuum tubes. Optical devices have tremendous merit over the vacuum tubes. In vacuum tubes and other electronic devices, the information transfer is carried out through electrons. However, optoelectronic devices depend on photons, an electrically neutral elementary particle. An electrically neutral photon in a communication line is exempt from electrical or magnetic fields associated with an electric current. Full electric isolation between the emitter and receiver is also accomplished by using optical devices. The introduction of the optical communication system eliminates the loss of information in transmission due to dissipation or accumulation of electrical charges. A broad group of optical devices such as photoresistors, photomultipliers, phototransistors, light-emitting diodes (LEDs), photodiodes (PDs), and lasers is used for information processing and transformation.

Light sources are one of the main components in the optoelectronics field. Although the initial research on optoelectronics started in 1955, swift development in the field occurred in the late 1960s after the invention of higher efficient means of interconversion of electrical and optical signals. The growth in the field of optoelectronics is assisted by the extensive use of light sources and optical fibers. Schubert indicated that the history of LEDs started when Round discovered electroluminescence in 1907 [3]. Though it was forgotten initially, scientists had started observing this phenomenon in later years. The LED, as we know now, has emerged only in the second half of the twentieth century. Advancement in the WBG semiconductor materials at the end of the 20th century leads to the development of optical devices operating in the ultraviolet-visible spectral region. Nitrides of group III elements attracted much attention from researchers working in the field of optical devices. One of the main properties of these elements, which makes them suitable for the optoelectronics field, is their direct bandgap. Materials such as GaN, aluminum nitride

(AlN), and indium nitride (InN) exhibit bandgap energy from 6.2 to 0.7 eV. Also, the possibility of bandgap engineering using group III alloys makes it ideal for applications in the ultraviolet-visible spectral region. By incorporating alloys, researchers were able to fabricate green, blue, and ultraviolet light sources and photodetectors.

The superior chemical properties of the group III – nitride elements are attributed to the strong chemical bonds due to the large difference in electronegativity between the group III and group V elements. Nitrides of group III elements possess a wurtzite structure and exhibits pyroelectricity, piezoelectricity, and second harmonic generation. The strong chemical bond between the elements gives the group III-nitrides a high melting point as well as chemical stability. The compounds exhibit a high thermal conductivity, which is suitable for effective heat dissipation in high-temperature applications. Also, the lower intrinsic carrier concentration of WBG material makes it an ideal candidate for high-temperature applications with low leakage current. A low reflectivity due to comparatively lower refractive indices makes group III-nitrides an excellent choice for the photodetector applications.

The GaN-based photoconductors are developed initially to avoid the complications caused by p-type doping of group III-nitride materials. The GaN-based photoconductors generally fabricated without the etching steps to define the device, which greatly simplified the fabrication process. It is reported that the photoconductors fabricated from group III-nitrides exhibit a gain over 3000 A/W. GaN-based Schottky diodes were also developed in the early decades of group III - nitride research due to the simplified fabrication process. Researchers were able to demonstrate Schottky diodes with low dark current and noise equivalent powers (NEP). Recent advances in the development of p-n and p-i-n junction diodes lead to high tailoring capability of cut-off wavelength by controlling the alloy incorporation. Also, the improvement in the material quality leads to the

development of more advanced group III-nitride photodiodes with lower noise interference, higher gains, and faster response, while keeping high flexibility on bandgap engineering.

In the early stages of the development of visible light emitters, researchers made use of indium gallium nitride-aluminum gallium nitride (InGaN/AlGaN) double-heterostructure to fabricate blue and green LEDs. Using double heterostructures, fabrication of high optical output LEDs were successful. However, one of the drawbacks of using double heterostructure is the broad spectrum linewidths. Green LEDs fabricated using double-heterostructure exhibits a spectrum range from violet to orange. To overcome this drawback, a single quantum well (SQW) structure is proposed. By using the SQW structure, researchers were able to fabricate LEDs with shorter spectrum line widths. When the double heterostructure exhibits a spectrum line width of 70 nm and optical output of 1 cd, the early SQW structure showed higher performance with a spectrum line width of 20nm and optical output of 12 cd. In the later years, the higher performance was achieved using strained quantum well, and multiple quantum well (MQW) designs.

Although the LEDs fabricated from group III-nitrides show significant advantages, some of the issues remain. The high-temperature operation of the LEDs is mainly restricted due to early failures. The early failures are supposed to be due to the high defect density. The instability of the InGaN active layer can also contribute to the early failure of group III-nitride LEDs. Due to the absence of a precise doping technology on group III-nitrides, LEDs fabricated based on group III-nitrides show a comparatively low breakdown voltage despite being considered as a WBG material. The current capability of the LEDs is also low compared to other WBG materials. Another critical issue that needs attention is the higher price for large volume applications. The fabrication cost of group III-nitride LEDs remains high as compared to other materials. Phosphorous coating on the blue LEDs to generate white light is not recommended in applications

where human interaction rate is high. It is observed that white LEDs from the combination of phosphorous and blue LEDs are not suitable for human eyes. Also, the efficiency of the phosphorous white LEDs is still lower compared to the fluorescent bulbs.

The development of lasers using group III-Nitride elements is a massive achievement in the research community. Much work has been done to achieve highly efficient laser diodes based on InGaN alloys. Blue and violet lasers fabricated from InGaN MQWs are demonstrated in the past. The lifetime and the power output of the laser diodes were significantly improved by adapting the lateral epitaxial growth mechanism to reduce the dislocation density. It is also reported that subsequent removal of substrate material leading to a free-standing GaN layer can also reduce the dislocation density. High series resistance is one of the major issues reported in the failure of GaN-based lasers. One of the solutions to achieve low series resistance is to have high p-type doping. However, the doping mechanism in the group III-nitride materials is still not understood very well. Also, more studies need to be conducted to identify the failure mechanism of GaN-based lasers.

1.3. Optical Integration Techniques in Power Electronics

Development of high voltage SiC power devices [4-16] and it's applications in emerging fields such as EM aircraft launch system (EMALS) [17], fly-by-light (FBL) systems [18,19], flexible ac transmission systems (FACTSs) [20] and solid-state power substation (SSPS) [21], calls for innovative techniques in the design of power modules and gate drive circuit. The gate driver design of a HV SiC power module should address various design challenges associated with the switching loss, electromagnetic (EM) emission and interference and dv/dt - di/dt stresses of power semiconductor devices (PSDs). Two primary functions of a medium voltage gate driver circuit include galvanically isolated signal transmission and power transmission [49]. Using optical isolation in signal and power transmission enable to overcome several design challenges

including external EM interference (EMI). Optical links also provide a reliable and inexpensive solution to conventional shielding and reduce the overall weight and volume of the application [22]. Optical isolation of the gate signal is realized by optocouplers [23] or optical fibers [24].

Optical fibers as a signal transmission path use an emitter and detector topology. This optoisolator-photodetector stage introduces an additional delay to the circuit. Also, these emitter-detector designs with optical fibers cannot modulate the switching dynamics of the PSD. Generally, modulation is done by a separate active gate control unit. By controlling the switching dynamics of the PSDs, one can control EM-noise generation, reduce the PSD dv/dt and di/dt stresses and switching losses [25, 26]. A possible solution to achieve switching dynamics modulation through optic links is by incorporating optically-activated power devices and replacing photodetectors. Earlier studies show the potential use of SiC devices as a photoconductive switch [27-29]. Several studies in the past decade introduced different optically activated discrete power devices [30-38][39-41].

A direct application (e.g., FBL) based optically triggered power device is first presented in [42]. It is important to note that it is not an ‘all SiC’ technology. The authors utilized the high light absorption efficiency of gallium arsenide achieve optically-triggered power transistor (OTPT). The same research team presented a series of hybrid designs, a combination of OTPTs and SiC power devices, after the success of initial studies [43]. Silicon carbide based optically-triggered thyristors is introduced in [44-46]. Although several optically triggered power devices are introduced in recent years, it is important to note that an ‘all SiC’ based gate drive system is still not presented yet.

Though optical links are widely used in gate signal isolation, the isolated gate-drive power supply is implemented with transformers [8, 14] until recently. In [47-49], an alternate solution for

isolated gate-drive power supply is presented using separated coils. Both transformers and separated coils are sensitive to EMI and require considerable space for isolation and shielding. Using fiber optic cables for carrying optical power, which is used as an energy source rather than carrying data, is first presented in [50,51]. Remotely powering of HV SiC devices and achieving electrical isolation at the same time is possible by this method. Optically isolated power transmission through optical fiber is presented in [25]. The proposed power over fiber (PoF)-based delivers sufficient gate drive power by laser light via optical fiber over a long distance (>1 m), and over 20-kV isolation voltage is achieved. However, the PoF method is not suitable for driving MOSFETs with paralleled dies as the maximum power output is limited to 0.5 W due to low efficiency (24%). An argument is also presented in [52], stating that the PoF is not reliable for the continuous operation of the converters. Other than isolation as a primary concern, optical fibers are also used as online IGBT junction temperature sensors (fiber Bragg grating) in energy conversion systems [53, 54].

1.4. Miniaturization Trend in Power Electronics

The application-driven miniaturization process of the power module highly depends on WBG materials such as SiC and GaN. The introduction of WBG materials in the fabrication of power modules helps achieve significant volumetric efficiency as compared with Si technology. The volumetric reduction of power modules is not only achieved by the smaller size of power semiconductor dies with high power density but also assisted by the required passive components, packaging, and cooling requirements. Figure 1.1 shows different stages involved in power system design. The power semiconductor research field is continuously evolving with the fabrication of devices with ever high voltage and current ratings. The power density of the devices is improved significantly by the development of higher quality substrate and epitaxial growth. However, the

volumetric reduction of the power module system now largely depends on other parts of the system, which consists of passives components and packaging technology itself. Rigorous research is underway in the high-temperature capability of passives and packaging technology to

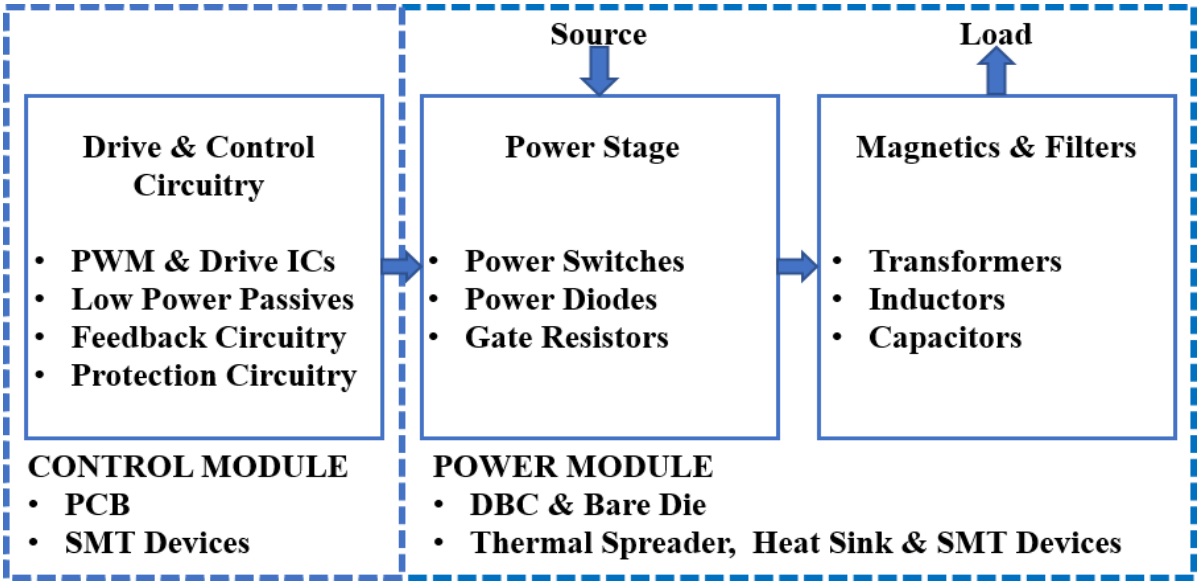

Figure 1.1. The different stages involved in a power system design.

successfully cop up with the temperature capability of power devices to achieve an ever-smaller design of power modules.

By developing high-quality SiC substrates, epitaxial layers, and selective doping, researchers were able to fabricate power semiconductor devices with minimum size for a given blocking voltage. Although this will effectively reduce the form factor of the power modules, designing suitable passive components is more important to fully utilize the benefits predicted by the use of WBG technology. The high switching speed of WBG power devices leads to the use of lower-valued inductors and capacitors with smaller form factors. However, tightly coupled passive components are necessary to avoid the effect of radiations emitted by the power devices. As compared to Si, the radiation effect on the passive components will be strong in WBG power devices. A much tightly coupled passive component design will ultimately lead to gate drivers placed close to switching devices. Integrating the gate driver and protection circuity to the power

module further reduces the form factor of the system. In this integrated power module, the low-voltage passive components of the gate driver and the protection circuitry are placed close to the power devices, making them exposed to similar environmental conditions as the power devices. The volumetric reduction of the integrated power modules is now limited by the passive components in the gate driver circuitry.

1.5. Motivation

Power modules based on WBG materials enhance reliability and considerably reduce cooling requirements that lead to a significant reduction in total system cost and weight. Although these innovative properties lead power modules to higher power density, some concerns still need to be addressed to take full advantage of WBG-based modules. To achieve a reduced parasitic effect, higher volumetric efficiency, and faster switching speeds in SiC-based high-temperature power modules, gate driver circuits needs to be placed as close to the power modules.

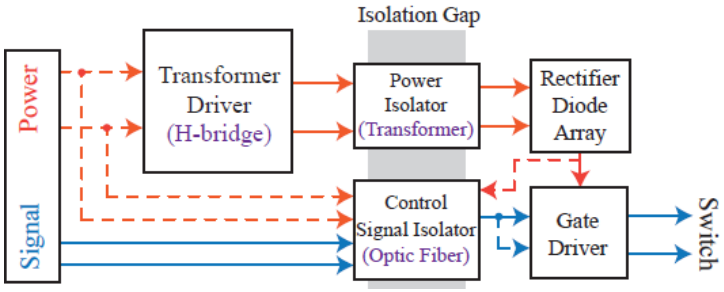

Figure 1.2. Schematic of a typical gate driver with isolation in both power and signal [50].

One of the main challenges in achieving high temperature integrated power module technology is the development of high-temperature passive components to go with the gate driver design. Figure 1.2 shows a schematic of a typical gate driver design. Most of the passive components, such as resistors, capacitors, and magnetics, are rated up to a maximum temperature

of 200^{o}C. Spyker et al. reported magnetic material capable of 300^{o}C operation. However, the magnetics, such as isolation transformers, are comparatively bulky and heavy in design. Typically, multiple transformers with large form-factor are used as the galvanic isolation system in power modules to float the high voltage gate driver. The modulation and demodulation circuits associated with the isolation transformers add to the complexity of gate driver design. Therefore, using isolation transformers of high form-factor limits scaling-down of power electronic modules. Table. 2 shows a comparison of optical isolation with the magnetic and capacitive coupling technique. A further scale down of power modules is possible by replacing bulky transformers with optocouplers of low form-factors. With the development of a suitable optical isolation system, i.e., optocouplers, volumetric issues associated with the magnetic isolation system can be avoided while simplifying the gate circuitry as well. However, the low performance of optoelectronic devices due to the degradation of quantum well efficiency, metallization, and packaging at high temperatures and

Table 1.2. Comparison of different galvanic isolation techniques.

Type of Isolations	***Coupling Method***	***Size & weight***	***Signal Modulating***	***Response Time***	***EMI /ESD***
Gate transformer	Magnetic	Bulky, heavy	Needed	Fast	Average
Digital isolation	Capacitive	Small, light	Needed	Medium	Average
Opto-coupler	Optical	Small, light	Not Needed	Medium	Good

operating conditions prevents the use of optocouplers in high-density power modules. A systematic study of the high-temperature operation of optoelectronic devices, i.e., emitters and photodiodes, is necessary to overcome the limiting factors in developing the high-temperature optocouplers. Thus far, a minimal reported study is available in the literature on the high-temperature application of optoelectronic devices.

The motivation for this study is the tremendous advantages in the energy-saving sector by the miniaturization of power systems. A detailed study on optoelectronic devices at high temperature enables us to explore the possibility of scaling high-density power modules by integrating high-temperature optoelectronic devices into the power module. The primary goal of this study is to characterize and verify the high-temperature operation of optoelectronic devices, including light-emitting diodes and photodiodes based on WBG materials. The secondary goal is to identify and integrate optoelectronic devices to achieve galvanic isolation in high-density power modules working at elevated temperatures. As part of the study, a high-temperature packaging, based on low temperature co-fired ceramic (LTCC), suitable to accommodate optoelectronic devices, will also be designed and developed.

1.6. Overview of the Dissertation

This dissertation is organized into 7 chapters. Chapter 1 reviews the current technology impact of the WBG materials on power electronic modules and optoelectronics. This chapter will also give insight to the readers about the current development in the field of optical integration to power electronics. By concluding the chapter by current development and future trends of power module miniaturization, the author identifies the problem statement and motivation for this work.

The chapters numbered three to six are based on peer-reviewed publications. The chapters are not necessarily in the chronological order in which they were published. The arrangement of the chapters aims to give the readers a thorough understanding of the product development process from material characterization, device optimization, high-temperature packaging, and final testing.

References

[1] N. Kaminski, "State of the art and the future of wide bandgap devices," 13th European Conference on Power Electronics and Applications, Barcelona, pp. 1-9, 2009.

[2] M. Kanechika, T. Uesugi, and T. Kachi, “Advanced SiC and GaN power electronics for automotive systems,” 2010 International Electron Devices Meeting, 2010.

[3] E. Schubert, “Light-emitting Diodes,” Cambridge University Press, 2003, pp. 55-70.

[4] V. Pala et al., “10 kV and 15 kV silicon carbide power MOSFETs for next-generation energy conversion and transmission systems,” in Proc. IEEE ECCE, Sep. 2014, pp. 449–454.

[5] M. K. Das et al., “10 kV, 120 A SiC half H-bridge power MOSFET modules suitable for high frequency, medium voltage applications,” in Proc. IEEE ECCE, Sep. 2011, pp. 2689–2692.

[6] S. Madhusoodhanan et al., “Solid-state transformer and MV grid tie applications enabled by 15 kV SiC IGBTs and 10 kV SiC MOSFETs based multilevel converters,” IEEE Trans. Ind. Appl., vol. 51, no. 4, pp. 3343–3360, Jul./Aug. 2015.

[7] K. Fukuda et al., “Development of ultrahigh-voltage SiC devices,” IEEE Trans. Electron Devices, vol. 62, no. 2, pp. 396–404, Feb. 2015.

[8] Kadavelugu et al., “Characterization of 15 kV SiC n-IGBT and its application considerations for high power converters,” in Proc. IEEE ECCE, Sep. 2013, pp. 2528–2535.

[9] D. Rothmund, G. Ortiz, T. Guillod, and J. W. Kolar, “10 kV SiC-based isolated DC-DC converter for medium voltage-connected solid-state transformers,” in Proc. IEEE APEC, Mar. 2015, pp. 1096–1103.

[10] Kadavelugu et al., “Medium voltage power converter design and demonstration using 15 kV SiC N-IGBTs,” in Proc. IEEE APEC, Mar. 2015, pp. 1396–1403.

[11] A. K. Tripathi et al., “Design considerations of a 15-kV SiC IGBT based medium-voltage high-frequency isolated DC–DC converter,” IEEE Trans. Ind. Appl., vol. 51, no. 4, pp. 3284–3294, Jul./Aug. 2015.

[12] K. Mainali et al., “A transformerless intelligent power substation:A three-phase SST enabled by a 15-kV SiC IGBT,” IEEE Power Electron. Mag., vol. 2, no. 3, pp. 31–43, Sep. 2015.

[13] S. Madhusoodhanan et al., “Performance evaluation of 15 kV SiC IGBT based medium voltage grid connected three-phase three-level NPC converter,” in Proc. IEEE ECCE, Sep. 2015, pp. 3710–3717.

[14] K. Vechalapu, A. Tripathi, K. Mainali, B. J. Baliga, and S. Bhattacharya,"Soft switching characterization of 15 kV SiC n-IGBT and performance evaluation for high power converter applications," in Proc. IEEE ECCE,Sep. 2015, pp. 4151–4158.

[15] A. Tripathi et al., "MVDC microgrids enabled by 15 kV SiC IGBT based flexible three phase dual active bridge isolated DC-DC converter," in Proc. IEEE ECCE, Sep. 2015, pp. 5708–5715.

[16] S. Madhusoodhanan et al., "Three-phase 4.16 kV medium voltage grid tied AC-DC converter based on 15 kV/40 A SiC IGBTs," in Proc. IEEEECCE, Sep. 2015, pp. 6675–6682.

[17] M. R. Doyle, D. J. Samuel, T. Conway, and R. R. Klimowski, "Electromagnetic aircraft launch system-EMALS," IEEE Trans. Magn., vol. 31,no. 1, pp. 528–533, Jan. 1995.

[18] J. R. Todd, "Direct optical control: A lightweight backup consideration," in Proc. IEEE Nat. Aerosp. Electron. Conf., 1992, vol. 2, pp. 456–463.

[19] S. K. Mazumder and T. Sarkar, "Optically-triggered power transistor(OTPT) for fly-by-light (FBL)/EMI susceptible power electronics," in Proc. IEEE Power Electron. Spec. Conf., 2006, pp. 1–8, Plenary Paper.

[20] W. H. Sew, Q. Li, M. G. Stewart, K.Walker, and C. Piner, "Measurement of electromagnetic emissions from FACTS equipment operational within substations—Part I," IEEE Trans. Power Del., vol. 20, no. 2, pp. 1775– 1881, Apr. 2005.

[21] A. Hefner, S.H.Ryu, B. Hull, D. Berning, C. Hood, J. M. Ortiz-Rodriguez,A. Rivera-Lopez, T. Duong, A. Akuffo, and M. Hernandez-Mora, "Recentadvances in high-voltage, high-frequency silicon-carbide power devices,"in Proc. IEEE Ind. Appl. Soc. Conf., 2006, pp. 330–337.

[22] S. Hazra, K. Vechalapu, S. Madhusoodhanan, S. Bhattacharya, andK. Hatua, "Gate driver design considerations for silicon carbide MOSFETsincluding series connected devices," in 2017 IEEE Energy ConversionCongress and Exposition (ECCE), Oct 2017, pp. 1402–1409.

[23] X. Zhang, H. Li, J. A. Brothers, J. Wang, L. Fu, M. Perales, and J. Wu,"A 15 kV SiC MOSFET gate drive with power over fiber based isolatedpower supply and comprehensive protection functions," in 2016 IEEEApplied Power Electronics Conference and Exposition (APEC), March2016, pp. 1967–1973.

[24] S. Park and T. M. Jahns, "Flexible dv/dt and di/dt control method forinsulated gate power switches," IEEE Trans. Ind. Appl., vol. 39, no. 3,pp. 657–664, May/Jun. 2003.

[25] P. J. Grvobic, "An IGBT gate driver for feed-forward control of turnonlosses and reverse recovery current," IEEE Trans. Power Electron.,vol. 23, no. 2, pp. 643–652, Mar. 2008.

[26] Xianyue Gu, Qiong Shui, Charles W. Myles and Martin A. Gundersen, “Comparison of silicon, galliumarsenide, silicon carbide and gallium nitride FET-type switches for pulsed power applications”, 14thInternational Pulsed Power Conference, 2003.

[27] W. Nunnally and M. Mazzola, “Opportunities for employing silicon carbide in high powerphoto-switches”, IEEE Pulsed Power Conference, Vol. 2, pp. 823 – 826, 2003.

[28] K.S. Kelkar, N.E. Islam, C.M. Fessler, and W. Nunnally, “Silicon carbide photoconductive switch forhigh-power, linear mode operations through sub-band-gap triggering”, Journal of Applied Physics, Vol.98 (093102), 2005.

[29] B.E. Danielsson, “HVDC vale with ligh triggered thyristors”,International Conference on AC and DC Power Transmission, pp. 159-164, 1991.

[30] R. L. Batdorf, A. G. Chynoweth, G. C. Dacey and P. W. Foy, “Uniform Silicon p–n Junctions. I. Broad Area Breakdown,”, Jrnl. Appl. Phys., vol. 31, no. 7, pp. 1153–1160, 1960, 10.1063/1.1736199.

[31] J.H. Hur, P. Hadizad, S.R. Hummel, P.D. Dapkus, H..R. Fetterman, andM.A. Gundersen, “GaAs opto-thyristor for pulsed power applications”,IEEE Conference Record of the Nineteenth Power ModulatorSymposium, pp. 325 – 329, 1990.

[32] J.H. Zhao, T. Burke, D., Larson, M. Weiner, A. Chin, J.M. Ballingall, T.Yu, M. Weiner, W.R. Buchwald, and K.A. Jones, “Sensitive opticalgating of reverse-biased AlGaAs/GaAs optothyristors for pulsed powerswitching applications”, IEEE Transactions on Electron Devices, vol.41, no. 5, pp. 809 – 813, May 1994.

[33] J.-L. Sanchez, R. Berriane, J. Jalade, and J.P. Laur, “Functionalintegration of MOS and thyristor devices: a useful concept to create newlight triggered integrated switches for power conversion”, FifthEuropean Conference on Power Electronics and Applications, vol. 2, pp.5-9, 13-16 Sep 1993.

[34] P. Hadizad, J.H. Hur, H. Zhao, K. Kaviani, M.A. Gundersen, and H.R.Fetterman, “A high-voltage optoelectronic GaAs static inductiontransistor”, IEEE Electron Device Letters, vol. 14, no. 4, pp. 190 – 192,1993.

[35] T. Yamagata and K. Shimomura, “High responsivity in integratedoptically controlled metal-oxide semiconductor field-effect transistorusing directly bonded SiO2 –InP”, IEEE Photonics Tech Letters, vol. 9,pp. 1143 -1145, 1997.

[36] M. Madheswaran, and P. Chakrabarti, “Intensity modulated photoeffectsin InP-MIS capacitors”, IEE proceedings on optoelectronics, vol. 143,pp. 248-251, 1996.

[37] T. Sarkar and S.K. Mazumder, “Amplitude, pulse-width, andwavelength modulation of a novel optically-triggered power DMOS”,accepted for 35th IEEE Power Electronics Specialists Conference PESC2004, Germany, June, 2004.

[38] A. Rosen, P. Stabile, W. Janton, A. Gombar, P. Basile, J. Delmaster, andR. Hurwitz, “Laser-activated p-i-n diode switch for RF application”,IEEE Transactions on Microwave Theory and Techniques, vol. 37, no.8, pp. 1255 – 1257, 1989.

[39] A. Rosen, P. Stabile, A.M. Gombar, W.M. Janton, A. Bahasadri, and P.Herczfeld, “100 kW dc biased, all semiconductor switch using Si pindiodes and AlGaAs 2-D laser arrays”, IEEE Photonics TechnologyLetters, vol. 1, no. 6, pp. 132 – 134, 1989.

[40] A. Madjar, A. Paolella, and P.R. Herczfeld, “Modeling the opticalswitching of MESFET's considering the external and internalphotovoltaic effects”, IEEE Transactions on Microwave Theory andTechniques, vol. 42, no. 1, pp. 62 – 67, 1994.

[41] S.K. Mazumder and T. Sarkar, ‘Optically-activated gate control forpower electronics’, IEEE Transactions on Power Electronics, vol. 26,no. 10, pp. 2863-2886, 2011.

[42] A. Mojab, S.K. Mazumder, L. Cheng, A.K. Agarwal, and C.J. Scozzie,“15-kV single-bias all-optical ETO thyristor”, IEEE InternationalSymposium on Power Semiconductor Devices, 2014.

[43] A. Meyer, A. Mojab, and S.K. Mazumder, “Evaluation of first 10-kVoptical ETO thyristor operating without any low-voltage controlbias”, IEEE International Symposium on Power Electronics forDistributed Generation Systems,DOI: 10.1109/PEDG.2013.6785592, 2013.

[44] A. Mojab and S.K. Mazumder, “First 15-kV single-bias all-optical SiC ETO Thyristor”, IEEE Energy Conversion Conference and Exposition,2014.

[45] K. Kusaka, K. Orikawa, J.-I. Itoh, K. Morita, and K. Hirao, “Isolationsystem with wireless power transfer for multiple gate driver suppliesof a medium voltage inverter,” in Proc. IPEC-Hiroshima-ECCE-ASIA,May 2014, pp. 191–198.

[46] S. Brehaut and F. Costa, “Gate driving of high power IGBT by wirelesstransmission,” in Proc. CES/IEEE 5th Int. Power Electron. MotionControl Conf. (IPEMC), Aug. 2006, pp. 1–5.

[47] K. Kusaka et al., “Galvanic isolation system for multiple gate driverswith inductive power transfer—Drive of three-phase inverter,” in Proc.IEEE ECCE, Sep. 2015, pp. 4525–4532.

[48] Fraunhofer ISE. (Jan. 2016). Power-by-Light. [Online]. Available: https://www.ise.fraunhofer.de/en/business-areas/photovoltaics/researchtopics/iii-v-and-concentrator-photovoltaics/fields-of-work/power-bylight/power-by-light

[49] J.-G. Werthen, “Powering next generation networks by laser lightover fiber,” in Proc. Conf. Opt. Fiber Commun./Nat. Fiber Opt. Eng.Conf. (OFC/NFOEC), Feb. 2008, pp. 1–3.

[50] A. Anurag, S. Acharya, Y. Prabowo, G. Gohil and S. Bhattacharya, "Design Considerations and Development of an Innovative Gate Driver for Medium Voltage Power Devices with High dv/dt," in IEEE Transactions on Power Electronics. doi: 10.1109/TPEL.2018.2870084

[51] Bazzo, J.P.; Lukasievicz, T.; Vogt, M.; de Oliveira, V.; Kalinowski, H.J.; da Silva, J.C.C. Thermal characteristicsanalysis of an IGBT using a fiber Bragg grating. Opt. Lasers Eng. 2012, 50, 99–103.

[52] Sousa, K.M.; Bazzo, J.P.; Mezzadri, F.; Bortolotti, F.; Martelli, C.; Silva, J.C.C.; Probst, W.K. Optical fiberBragg grating sensors applied on energy conversion systems. In Proceedings of the 2013 SBMO/IEEE MTT-SInternational Microwave & Optoelectronics Conference (IMOC), Rio de Janeiro, Brazil, 4–7 August 2013;pp. 1–5.

[53] R. Newman, “Visible light from a Silicon p-n junction,”, Phys. Rev., vol. 100, no. 2, pp. 700–703, 1955, 10.1103/PhysRev.100.700.

[54] A. G. Chynoweth and K. G. McKay, “Light Emission and Noise Studies of Individual Microplasmas in Silicon p–n Junctions,”, Jrnl. Appl. Phys., vol. 30, no. 11, pp. 1811–1813, 1959, 0.1063/1.1735060.

2. Electro-optical Characterization Bench

2.1. Quantum Efficiency Extraction of LEDs

The optoelectronic device characteristics at high temperatures highly depend on materials of active layers and substrate, device structures, processes, packaging, and operating conditions. Optoelectronic devices made from wide bandgap compound semiconductors are an immediate choice for high-temperature applications due to the unique characteristics of wide bandgap materials, such as less degradation at high temperature, inherent radiation hardness, excellent thermal conductivity, and high breakdown field. Advanced electroluminescence (EL) measurement system is built to characterize LED devices at high temperatures (up to 800K). The schematic of the EL measurement system is shown in Figure 1. The EL set up consists of a Horiba iHR 550 (Kyoto, JA www.horiba.com) spectrometer with attached liquid nitrogen (LN)

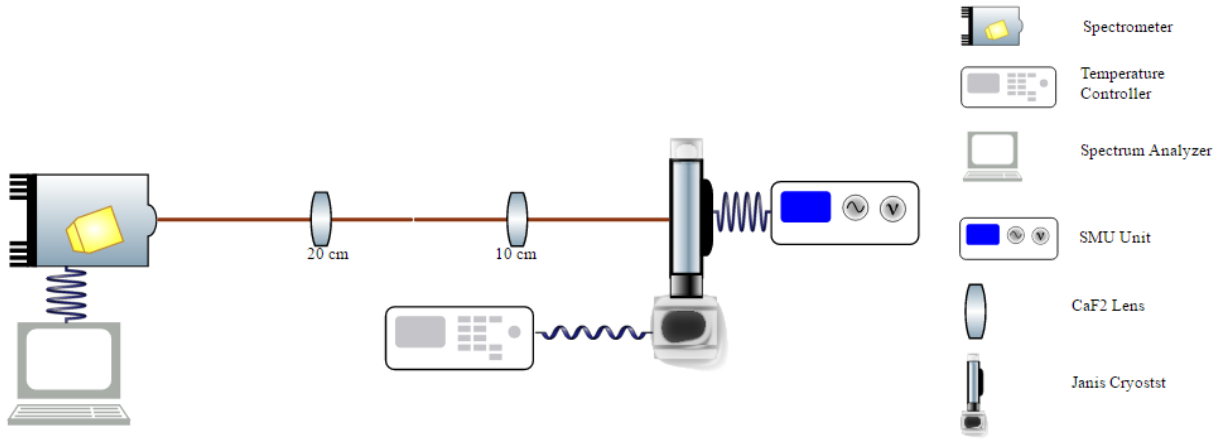

Figure 2.1. Schematic drawing of the high temperature EL system

cooled charge-coupled device (CCD) camera. The temperature of the CCD camera was kept under 150 K during the measurements. A Janis ST-100H cryostat is integrated into the set up to have

temperature-dependent measurements. The high-temperature cryostat system consists of a cold finger, radiation shield, sample holder, lightweight aluminum vacuum shroud, electrical feed-through ports, and a high efficiency flexible six-foot cryogen transfer line. The temperature of the sample is varied by means of a heater attached to the cold finger. The sample mount and all standard sample holders have provisions for thermometry, which in conjunction with a temperature controller. The temperature controller allows precise control over the sample temperature up to 0.1K. High power heaters provide sample temperatures up to 800K.

The internal quantum efficiency (IQE) of the LEDs is calculated based on the power-law relationship between the injection current and the light output power from the temperature- and intensity-dependent electroluminescence (T-IDEL) measurements. Based on the power-law relationship in EL measurements, the electron-hole pair photoexcitation density is proportional to the current injection density, J_{EL}. In addition to that, the spontaneous emission rate per unit area per unit length from the active region is proportional to the EL signal integrated over energy, L_{EL}. The relationships are described by:

$$J_{EL} = \frac{c_a}{\eta_{inj}}[An + (1-\gamma_r)Bn^2 + Cn^3]\ ;\ L_{EL} = c_b\eta_{ext}Bn^2 \propto P_{out} \qquad (1)$$

where c_a and c_b are constants of proportionality determined by sample and measurement geometry. P_{out} is the light output power from the LED. The current injection efficiency and the light extraction efficiency of the LED are denoted by η_{inj} and $\eta_{ext,}$ respectively. For this study, the photon recycling factor, γ_r, is assumed to be independent of the current injection density. The recombination coefficients for the Shockley-Reed-Hall (SRH), radiative, and Auger mechanisms are denoted by A, B, and C, respectively. The recombination rates are presented as powers of the electron-hole concentration n.

The injection current density J_{EL} can be expressed as a function of L_{EL} from Eq. (1) as

follows:

$$J_{EL} = A_{EL}{L_{EL}}^{1/2} + B_{EL}L_{EL} + C_{EL}{L_{EL}}^{3/2} \quad (2)$$

where A_{EL}, B_{EL}, and C_{EL} are the best-fit parameters calculated by fitting Eq. (2) to the experimental data.

The internal quantum efficiency of the LED is defined as:

$$\eta_{IQE} = \frac{Bn^2}{An + Bn^2 + Cn^3} \quad (3)$$

Using Eq. (1) & (2), internal quantum efficiency can be expressed as:

$$\eta_{IQE} = \left(1 + \frac{A_{EL}}{B_{EL}}\left(\frac{1-\gamma_r}{\sqrt{L_{EL}}}\right) + \frac{C_{EL}}{B_{EL}}(1-\gamma_r)\sqrt{L_{EL}}\right)^{-1} \quad (4)$$

The external quantum efficiency (EQE), η_{EQE}, of the LED is defined using the relationship:

$$\eta_{EQE} = qP_{out}/I\hbar\omega \quad (5)$$

where q is the electron charge, and $\hbar\omega$ is the photon energy. The EQE is expressed as a function of integrated EL intensity using Eq. (1):

$$\eta_{EQE} \propto qL_{EL}/I\hbar\omega \quad (6)$$

Equation (6) enables us to calculate normalized EQE from T-IDEL measurements.

2.2. Spectral Response Measurements

Figure 2.2 shows the schematic of the high-temperature spectral response set up for detectors. The actual picture of the measurement setup is shown in Fig. 2.3. Temperature-dependent measurements were performed using a Janis ST-100H cryostat with an LN cooling and temperature controller. The devices were placed inside the cryostat using a chip carrier, and electrical connections were made using a BNC feed-through system. The spectral responses of the

structure were obtained using a tunable monochromator. The monochromator houses a 250W, 24V tungsten halogen lamp for wavelengths from 450 nm – 900 nm and a deuterium lamp for

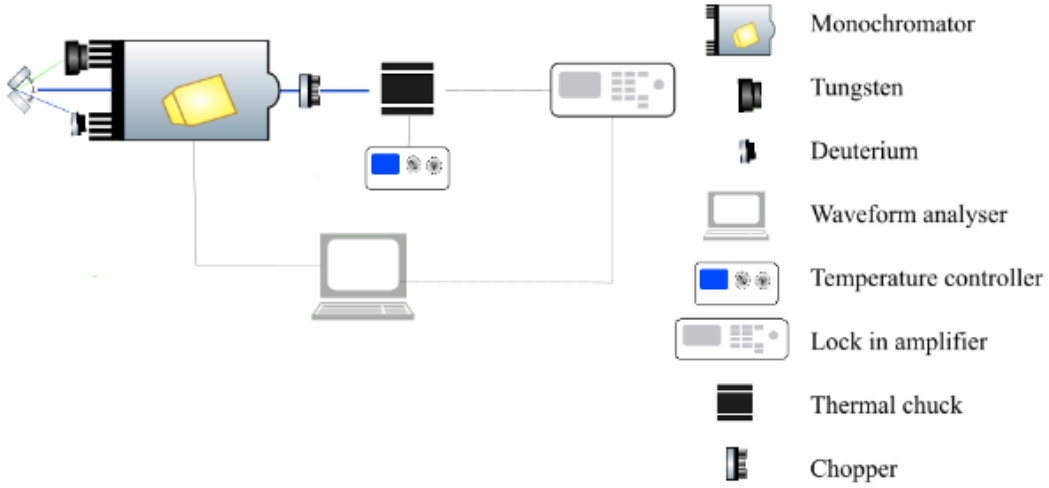

Figure 2.2. Schematic drawing of the high temperature spectral response system.

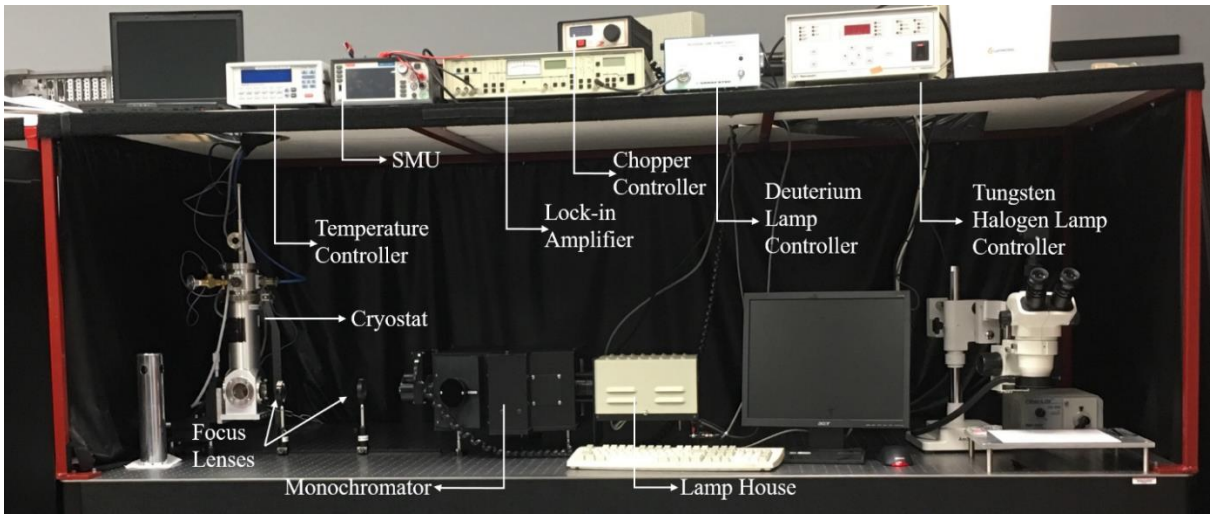

Figure 2.3 High temperature spectral response measurement setup

wavelengths from 190 nm – 450 nm. A calibrated Si detector is used to measure the incident power on the sample structure from the monochromator. The dimension of the calibrated Si detector is 3.6 mm × 3.6mm.

Both DC and AC measurements were conducted on the sample. During the DC measurements the device under test (DUT) was illuminated at different wavelengths and the current was read directly from Keithley SMU. In DC measurements the photocurrents were obtained by subtracting the dark current from the measured currents. However, at high temperatures, the dark current predominates the photocurrents and the detection was not possible. To overcome this difficulty, AC measurements were introduced. In AC measurements, the DUT was illuminated using chopped light at different wavelength and the photocurrent was read from lock-in amplifier. AC measurements were performed by incorporating chopper and lock-in amplifier.

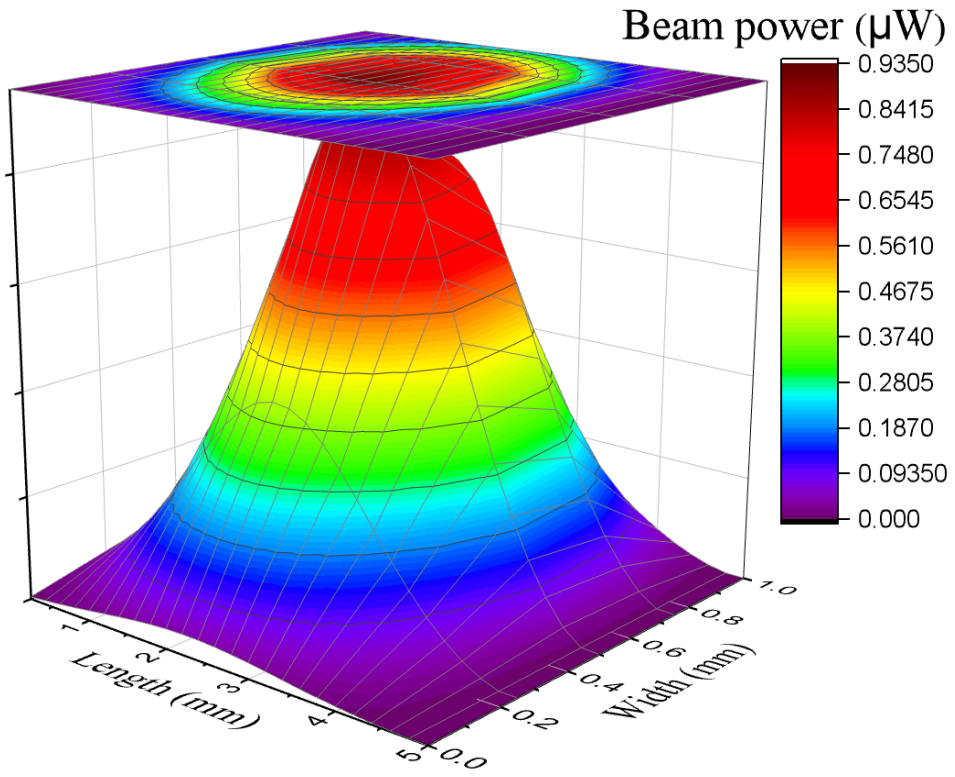

Figure 2.4. 3D graphing of the beam profile of the Tungsten halogen lamp at 535 nm.

The dimension of the beam spot at the plane of focus (PoF) is roughly 1mm × 5mm. Since the sample devices were smaller than the PoF, beam profiling was necessary. The beam profiling was carried out at different wavelengths. A calibrated Si detector is used to calculate the beam power. We also used a calibrated IXL lightwave power meter to verify the beam profiling at 450, 535, and 630nm. Table. 2.1 shows the beam power at different wavelengths measured using calibrated Si photodetector and IXL lightwave power meter. By using a detector with a smaller dimension than the PoF along with a 3D stage, we accurately profile the beam spot. Figure 2.4 shows the 3D surface image of the beam spot at 535nm. The 2D image of the beam profile is

shown in Fig 2.5. The beam profiling was repeated for different wavelengths to calculate the beam power.

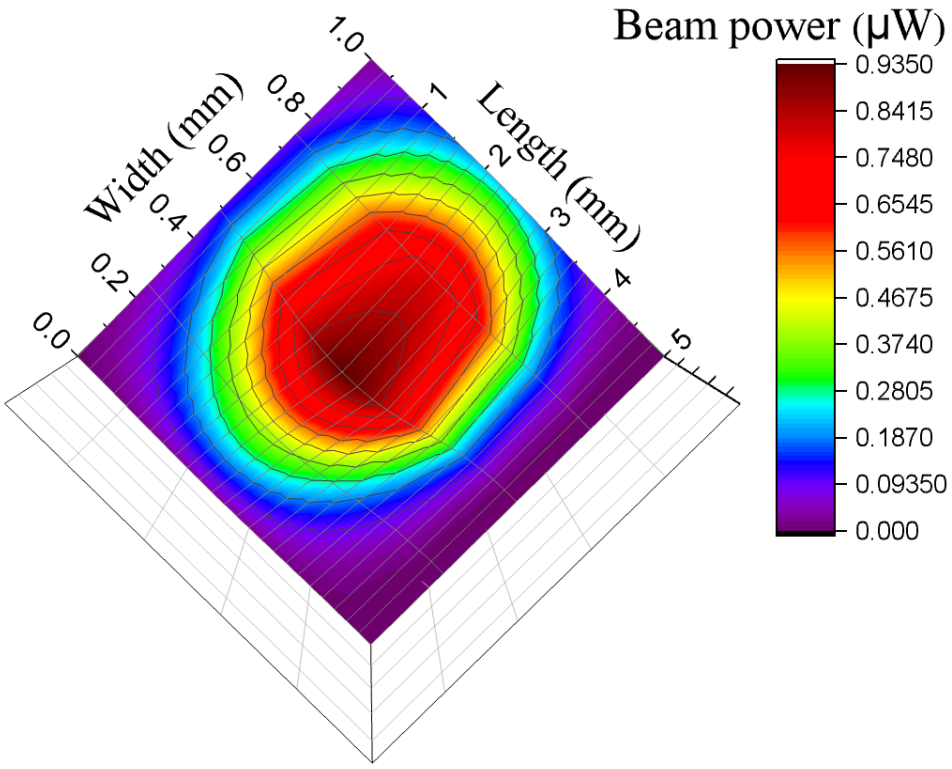

Figure 2.5. 2D surface graphing of the beam profile of the Tungsten halogen lamp at 535 nm.

Table 2.1. The measured beam powers for different wavelengths

Wavelength (nm)	***Measured power (μW)***	
	Calibrated Si	***IXL power meter***
450	46.44 μW	48.1 μW
535	28.14 μW	29.79 μW
630	9.51 μW	9.6 μW

The photocurrents were measured using a lock-in amplifier based on which the responsivity, $\Re$, is extracted. A Keithley 236 source measurement unit (SMU) was used to measure the dark current-voltage (I-V) characteristics in the temperature range 77 -800 K.

The photodetector sensitivity of the structure is quantified using the material figure of merit parameter D*, calculated in units of Jones (cm $Hz^{1/2}W^{-1}$), as below:

$$D^* = \frac{\sqrt{A\Delta f}}{i_{rms}}\Re \tag{1}$$

where A is the active detecting area of the structure in square centimeter, Δf is referred to the equivalent noise bandwidth (ENBW) in hertz, $\Re$ is the spectral responsivity in ampere per watt, and i_{rms} is the root mean square of noise currents in the detector system. In this study, Δf is taken as 1 Hz. The i_{rms} , which includes Johnson or thermal noise, shot noise, generation-recombination noise, and 1/f noise, is calculated as follow:

$$i_{rms} = \sqrt{i_{thermal}^2 + i_{shot}^2 + i_{G-R}^2 + i_{1/f}^2} \tag{2}$$

The generation-recombination noise occurred due to the random generation, and the recombination of free carriers caused by crystal vibrations is considered as zero in this study as this occurs mainly in photoconductors and is limited by diffusion in an ideal photodiode. Also, 1/f noise or flicker noise is eliminated in this study as the noise level is negligible for detector works under high frequency. The thermal and shot noise is calculated using the following equations:

$$i_{thermal} = \sqrt{4kT\Delta f/R_0} \;\; ; \; i_{shot} = \sqrt{2qI\Delta f} \tag{3}$$

where k is the Boltzmann constant, T is the absolute temperature, R_0 is the resistance of the device, q is the charge of an electron, and I is the average current flow in the device under illumination, which includes both photocurrent and dark current. In this study, noise bandwidth was set by configuring the time constant and slope/oct of the lock-in amplifier to 100 ms and 18 dB/oct, respectively.

The device figure of merit, noise equivalent power (NEP), i.e., the minimum impinging optical power that a detector can distinguish from noise, is calculated as follows:

$$NEP = i_{rms} / \Re \tag{4}$$

Also, the D^* is related to NEP as follows:

$$D^* = \frac{\sqrt{A\Delta f}}{NEP} \tag{5}$$

3. High-Temperature Analysis of GaN-based Blue LEDs for Future Power Electronic Applications

3.1. Abstract

Commercial gallium-nitride-based blue light-emitting diodes (LEDs), primarily fabricated for lighting applications, are evaluated at high temperatures (up to 700 K) for possible integration as an optocoupler emitter in high-density power electronic modules. The temperature- and injection-current-dependent internal quantum efficiency and current-voltage characteristics of the blue LEDs are studied. The internal quantum efficiency (IQE) is extracted from the measured integrated electroluminescence (EL) intensity at different temperatures using the ABC model. The presented method helps evaluate the optimized injection current density to achieve minimum deviation in LED IQE at a broader range of operating temperatures. As per the ABC model, the LED can operate at 700 K with an IQE of 58.50% when it operates at a current density of 2A/cm2. The results show that for a temperature range of 77 – 700 K, the minimum deviation of IQE occurs when the injected current density is between 1 to 10 A/cm^2. Normalized external quantum efficiency (EQE) of the device at different temperatures were also extracted using the ABC model.

3.2. Introduction

Silicon carbide (SiC), a wide bandgap semiconductor with thermal conductivity over three times of that of silicon, drives the development of next-generation power electronic system suitable for high voltage and extreme temperature operation. Advancement in SiC device technology helps contribute to the development of a high-density power module, a fundamental component in power electronic system, for size- and weight-sensitive applications such as electric vehicles, motor

drives, and space exploration. Although power electronic modules achieved high scalability in the past two decades with the introduction of SiC technology, there are some power module components in the gate driving circuits such as isolation transformers that limit further size reduction. Isolation transformers are used where the devices are in series strings or devices that are on the high side require floating power supplies for the gate drive, and the signals required to trigger the devices must be isolated.

Typically, multiple transformers (i.e., each floating device requires a separate isolation transformer) with a large form-factor are used as a galvanic isolation system in power modules to float the high voltage gate driver. Bulky and heavy isolation transformers are often replaced with discrete optocouplers in conventional silicon power electronic modules with a targeted operating temperature up to 125 ^{o}C. However, SiC power modules designed to work at extreme conditions require high-temperature optocouplers to replace isolation transformers successfully. Therefore, the development of high-temperature optocouplers, which can be operated at an elevated temperature (e.g., 250 ^{o}C) with an extended lifetime, requires a systematic study of optoelectronic materials and devices at high temperatures.

We previously reported a systematic study of direct bandgap InGaN/GaN multiple quantum well (MQW) green optoelectronic material with a peak wavelength of 516 at room temperature as a part of the development of a high-temperature optocoupler [1]. The study shows that the spontaneous emission quantum efficiency (QE) of green LED epitaxy material at 527oC is around 44 %. A 44 % IQE is not suitable for lighting applications. However, it can be accommodated in the design of the optocoupler emitter application as long as the photodetector is not degraded in the optocoupler. The photoluminescence study on the materials shows that QE degradation with respect to temperature is also related to the injected laser power [1]. These

promising results lead to the characterization of commercial InGaN based LED devices to evaluate the possibility of operating at high temperatures and to determine the optimal current density to achieve peak IQE at different temperatures.

Since the commercially available LED devices are primarily designed for lighting and display applications where the application temperature usually does not exceed 150 oC, a drop in QE is expected at elevated temperatures due to non-optimized current injection at high temperatures. Even though our previous study has demonstrated the high-temperature capability of commercial LED materials, the LED devices' performance (i.e., IQE & EQE) also need to be understood. While the EQE of LED devices at high temperatures mainly depends on the device geometry, metallization, and packaging, IQE is strongly related to the injected current level and quantum well structure [2-4]. High injected current levels can also shorten the lifetime of LED devices. To develop the high-temperature optocouplers, which can be operated at 250 ^{o}C with at least ten-year lifetime, the trade-off between the IQE and device lifetime at different temperatures need to be understood. Therefore, a thorough study of LED devices at elevated temperatures is necessary to check the feasibility of LEDs implemented as the emitters in high-temperature optocouplers.

In this paper, we evaluate commercial InGaN/GaN MQW blue LEDs as potential candidates in high-temperature optocouplers due to their unique properties such as wide bandgap, low heat dissipation, and higher operating lifetime compared to gallium arsenide (GaAs) or gallium phosphide (GaP) based LEDs [5],[6]. To avoid the degradation of the devices due to the packaging, commercial bare-die LED devices are characterized to analyze the temperature-dependent and injected-current-dependent IQE. The reported high-temperature-dependent characterization of GaN-based LEDs focuses mainly on lighting applications [7-9]. In contrast,

this paper analyzes the temperature dependence of the LED performance focusing on the possibility to be integrated into high-density power modules. High-temperature analysis of the LEDs was conducted using temperature and injected current dependent EL. The IQE of the LEDs were extracted using the ABC model. The IQE as a function of injected current density is studied in detail for the optimization of LED injected current to achieve minimum deviation in IQE at higher temperatures. Normalized EQE of the LED is also calculated and presented. This investigation helps evaluate the feasibility of commercial LEDs as the emitter in the optocoupler to be operated at high temperatures.

3.3. Experiment

High-temperature optical and electrical studies were conducted on vertically-structured bare die blue LEDs manufactured by Cree Inc. Bare-die devices are selected to avoid unwanted failures at elevated temperatures due to the degradation of packaging media or forming lenses on the chip surface. The GaN-based blue LED structures were grown on SiC substrate. Both contact layers were formed by highly-reflective electrodes. A Horiba 550 spectrometer integrated with a photomultiplier tube (PMT) and a Janis ST-100H cryostat is used for temperature- and intensity-dependent electroluminescence (T-IDEL) measurements [10]. The cryostat was tuned and calibrated at each temperature to avoid any possible measurement error due to the thermal shift of the sample holder in the cryostat. Comparatively lower injection current levels were used to avoid LED failure due to self-heating. The LEDs were characterized up to 700 K due to the limitation of experiment setup to accurately capture enough EL data points at higher temperatures for IQE extraction. Keithley 2450 source measurement unit (SMU) is used to measure the current-voltage (I-V) characteristics of the LEDs.

The IQE is calculated based on the power-law relationship between the injection current

and the light output power from the T-IDEL measurements. Based on the power-law relationship in EL measurements, the electron-hole pair photoexcitation density is proportional to the current injection density, JEL. In addition to that, the spontaneous emission rate per unit area per unit length from the active region is proportional to the EL signal integrated over energy, L_{EL}. The relationships are described by:

$$J_{EL} = \frac{c_a}{\eta_{inj}}[An + (1-\gamma_r)Bn^2 + Cn^3]\ ;\ L_{EL} = c_b\eta_{ext}Bn^2 \propto P_{out} \tag{1}$$

where c_a and c_b are constants of proportionality determined by sample and measurement geometry. P_{out} is the light output power from the LED. The current injection efficiency and the light extraction efficiency of the LED are denoted by η_{inj} and $\eta_{ext,}$ respectively. For this study, the photon recycling factor, γ_r, is assumed to be independent of the current injection density [11]. The recombination coefficients for the Shockley-Reed-Hall (SRH), radiative, and Auger mechanisms are denoted by A, B, and C, respectively. The recombination rates are presented as powers of the electron-hole concentration n.

The injection current density J_{EL} can be expressed as a function of L_{EL} from Eq. (1) as follows:

$$J_{EL} = A_{EL}{L_{EL}}^{1/2} + B_{EL}L_{EL} + C_{EL}{L_{EL}}^{3/2} \tag{2}$$

where A_{EL}, B_{EL}, and $C_{EL}$are the best-fit parameters calculated by fitting Eq. (2) to the experimental data.

The internal quantum efficiency of the LED is defined as:

$$\eta_{IQE} = \frac{Bn^2}{An + Bn^2 + Cn^3} \tag{3}$$

Using Eq. (1) & (2), internal quantum efficiency can be expressed as:

$$\eta_{IQE} = \left(1 + \frac{A_{EL}}{B_{EL}}\left(\frac{1-\gamma_r}{\sqrt{L_{EL}}}\right) + \frac{C_{EL}}{B_{EL}}(1-\gamma_r)\sqrt{L_{EL}}\right)^{-1} \tag{4}$$

The external quantum efficiency (EQE), η_{EQE} , of the LED is defined using the relationship:

$$\eta_{EQE} = qP_{out}/I\hbar\omega \quad (5)$$

where q is the electron charge, and $\hbar\omega$ is the photon energy. The EQE is expressed as a function of integrated EL intensity using Eq. (1):

$$\eta_{EQE} \propto qL_{EL}/I\hbar\omega \quad (6)$$

Equation (6) enables us to calculate normalized EQE from T-IDEL measurements.

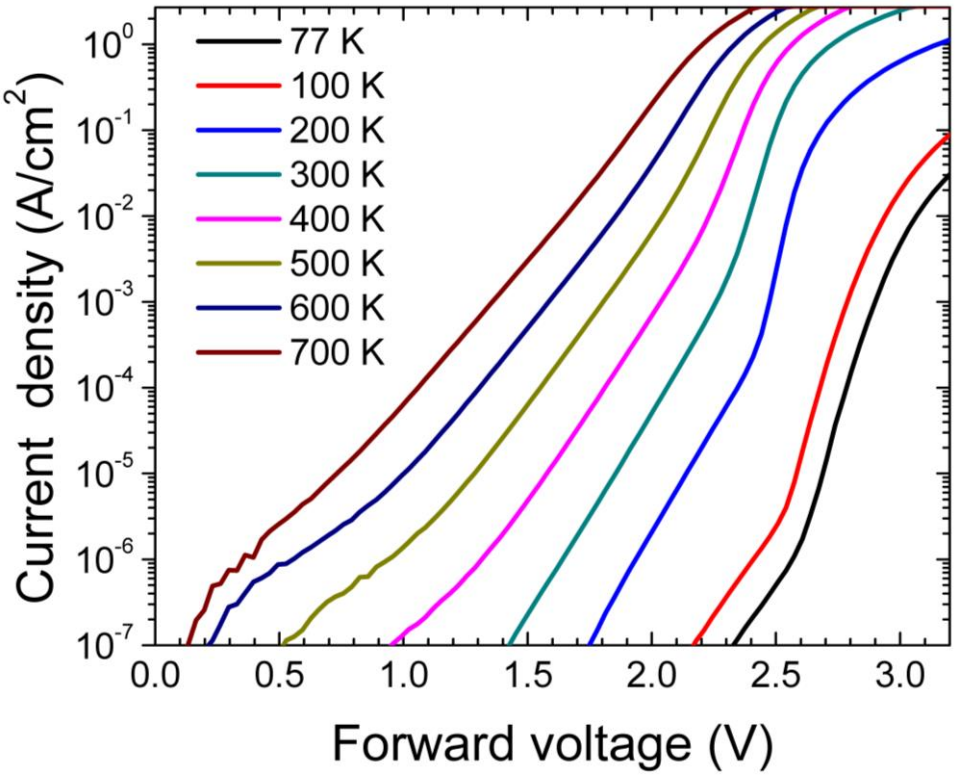

Figure 3.1. I-V characteristics of GaN based LED measured at different temperatures ranging from 77 - 700 K.

3.4. Results and Discussions

The current-voltage (IV) characteristics of the LED at a forward biased condition in the temperature range of 77 – 700 K are shown in Fig. 3.1. The I-V characteristics reveal a low current and high current region with a visible change in slope. The LED series resistance and current-

dependent p-n junction resistance determines the slope at the high-current region. The low current region, typically before the turn-on of the device, is present due to the trap-assisted tunneling of electrons and holes through midgap electronic states or carrier leakage via extended defects. The low current sections do not contribute to the radiative recombination of electrons and holes in the active region, thus creating carrier loss, which is not accounted for with the ABC model. The ABC model can be modified to account for this non-radiative recombination [12]. However, this is unnecessary as the injected current selected in our research is well above the low-current region.

The temperature-dependent EL spectra of the LED at an injection current of 10 mA is shown in Fig. 3.2. The inset of the figure shows the evolution of peak energy with respect to the temperature. The EL peak energy exhibits a weak S-shaped behavior over the temperature range

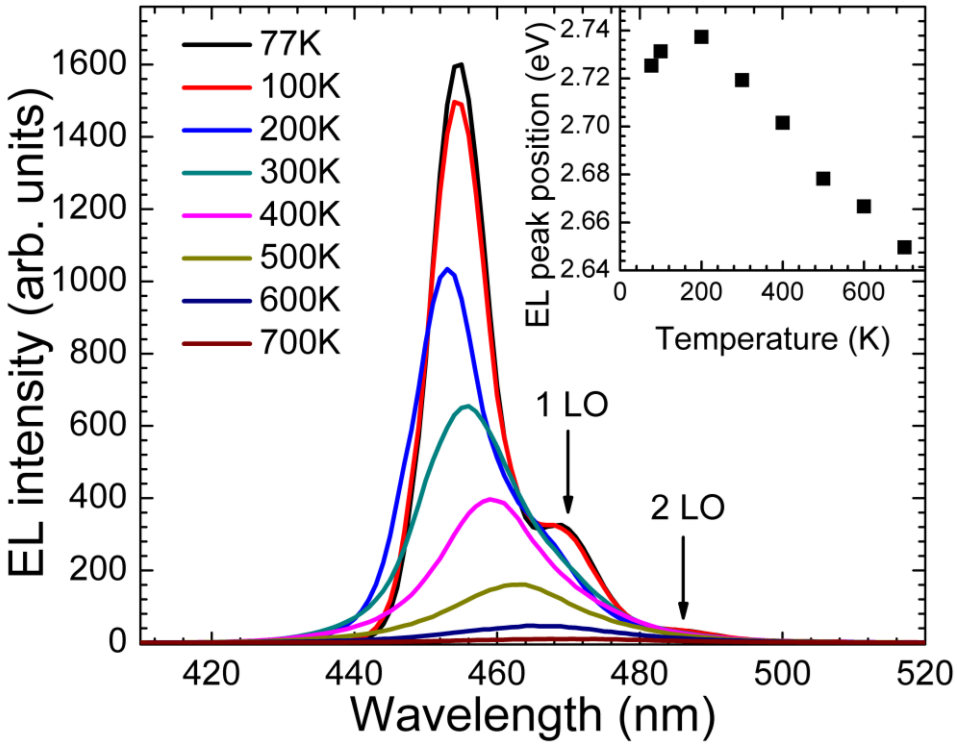

Figure 3.2. EL spectra of GaN-based LED measured at different temperatures. Arrows show the spectral positions of phonon replicas. Inset shows the evolution of EL peak position with temperature.

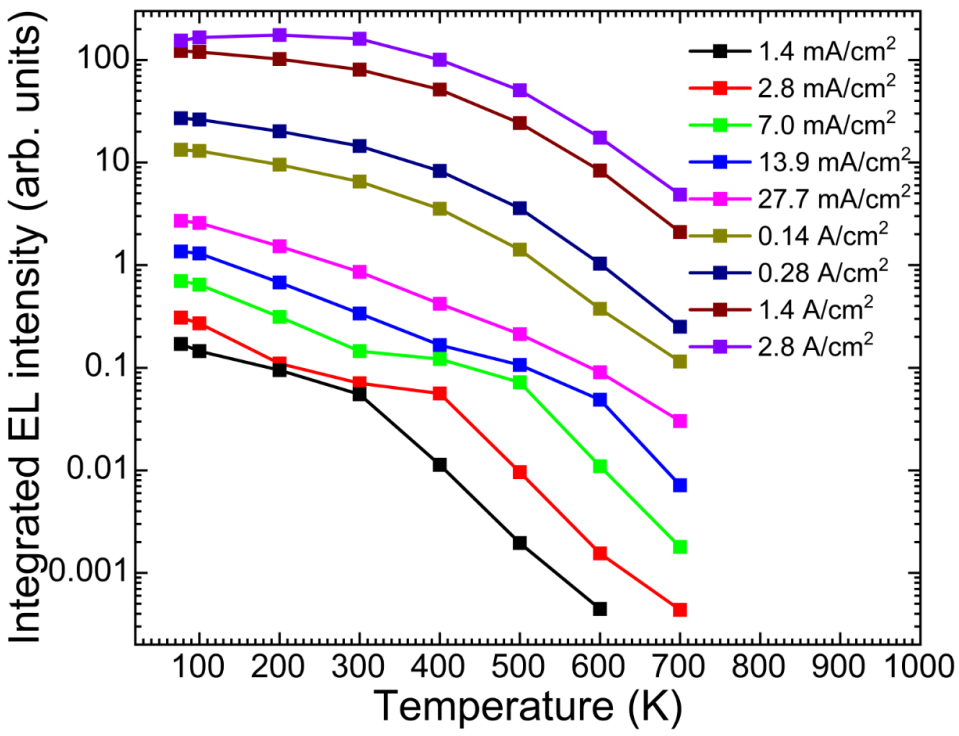

Figure 3.3. Integrated EL intensity as a function of temperature is calculated for different injected current densities.

77 – 700 K. First, the peak energy shows a blue shift from 2.72 eV at 77 K to 2.74 eV at 200 K, and then it started red-shifting at temperatures above 200 K. This behavior is typically attributed to carrier localization [13],[14]. The pronounced phonon replicas of the EL spectra at low temperatures are indicative of the high quality of the LED MQW structures. The phonon replicas are merged to the main band-to-band transitions at higher temperatures. The EL intensity of the LED dropped when the temperature increases from 77 – 700 K. Figure 3.3 shows the evolution of integrated EL intensity with respect to temperature for different injected current density. It is observed that as the injected current density increases, the percentage change in the EL intensity at different temperatures decreases. It suggests that selecting a higher injected current can reduce the percentage drop of the integrated EL intensity of the LED working at different temperatures. However, selecting a higher value of injected current can cause the LED to fail due to self-heating.

An optimized value of LED injected current for working at different temperatures can be calculated from the quantum efficiency measurements.

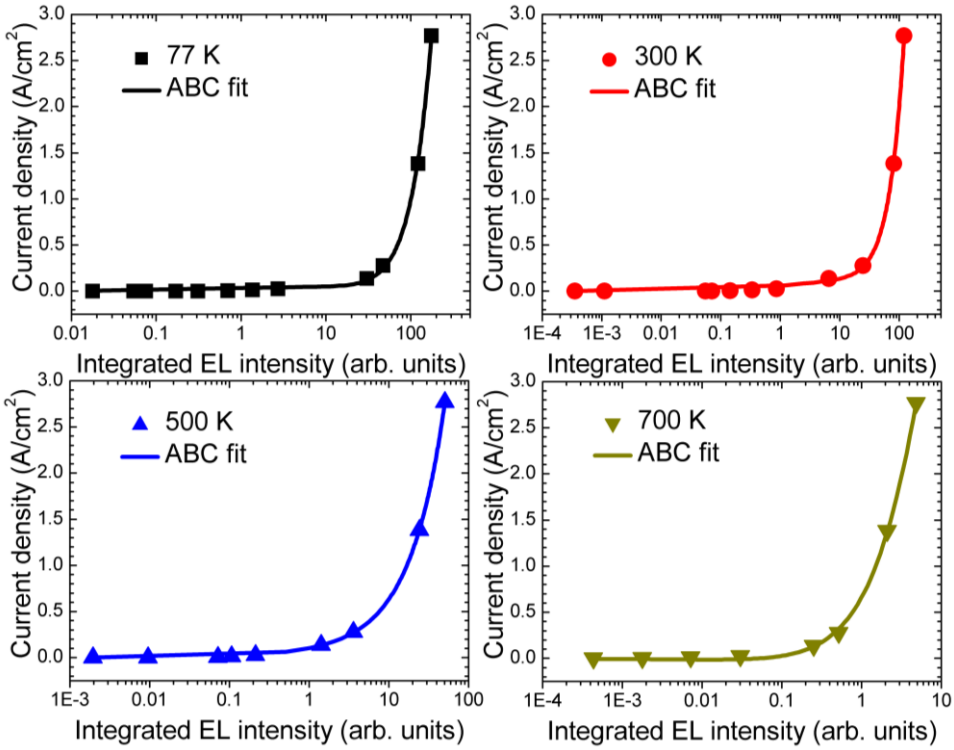

Figure. 3.4. Integrated EL intensity as a function of current density for different temperatures. The dots are the experimental results and the solid lines are fits to Eq. (2).

The fitting parameters A_{EL}, B_{EL}, and C_{EL} for the calculation of IQE are calculated by fitting Eq. (2) to the experimental data. Integrated EL intensity as a function of current density is plotted in Fig. 3.4 to obtain the different fitting parameters. The dots are the experimental results, while the solid lines are the fits to Eq. (2). The fit parameters extracted from Fig. 4 are used to calculate the IQE at different temperatures, which is plotted as a function of current density in Fig. 3.5. The IQE shows a dome-like shape, with the width gradually decreasing at higher temperatures. The sample shows a maximum IQE of 97.40% at 77 K. The IQE of the sample dropped to 58.50% at 700 K as per the ABC model. Figure 5 shows the evolution of IQE with respect to the injected current. The results show that a minimum deviation of IQE occurs when the injected current

density is between 1 to 10 A/cm^2.

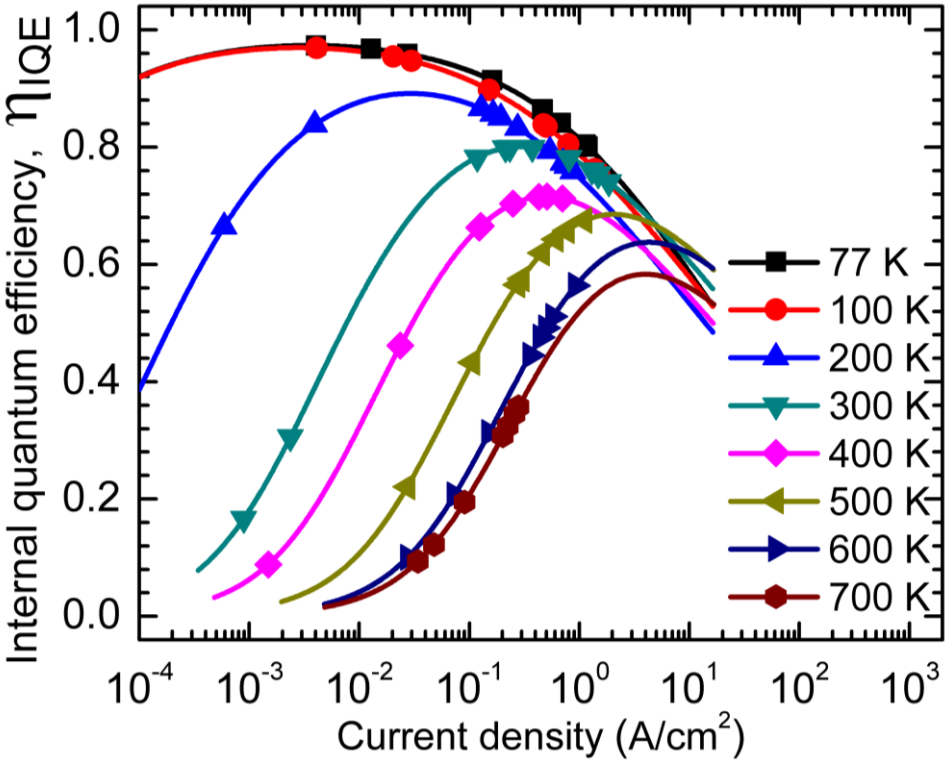

Figure 3.5. Internal quantum efficiency plotted as a function of current density at different temperatures.

The evolution of the thermal droop over different injection current can be explained using the carrier rate equation model [15]. The sample shows significant thermal droop at injection current densities below 1.0 mA/cm^2. The SRH recombination causes the thermal droop at low injection current densities. The SRH recombination contributes 47 % of the total recombination at an elevated temperature as compared to 10 % at 300 K [16]. However, at high injection levels (i.e., above 2 A/cm^2), the SRH recombination accounts for less than 3 % of the total recombination. Therefore, the thermal droop at high current injection is due to the Auger recombination and drift-induced carrier leakage. At moderate injection levels, radiative recombination becomes significant and leads to a reduction in the thermal droop.

Figure 3.6 shows the normalized EQE as a function of current density for different

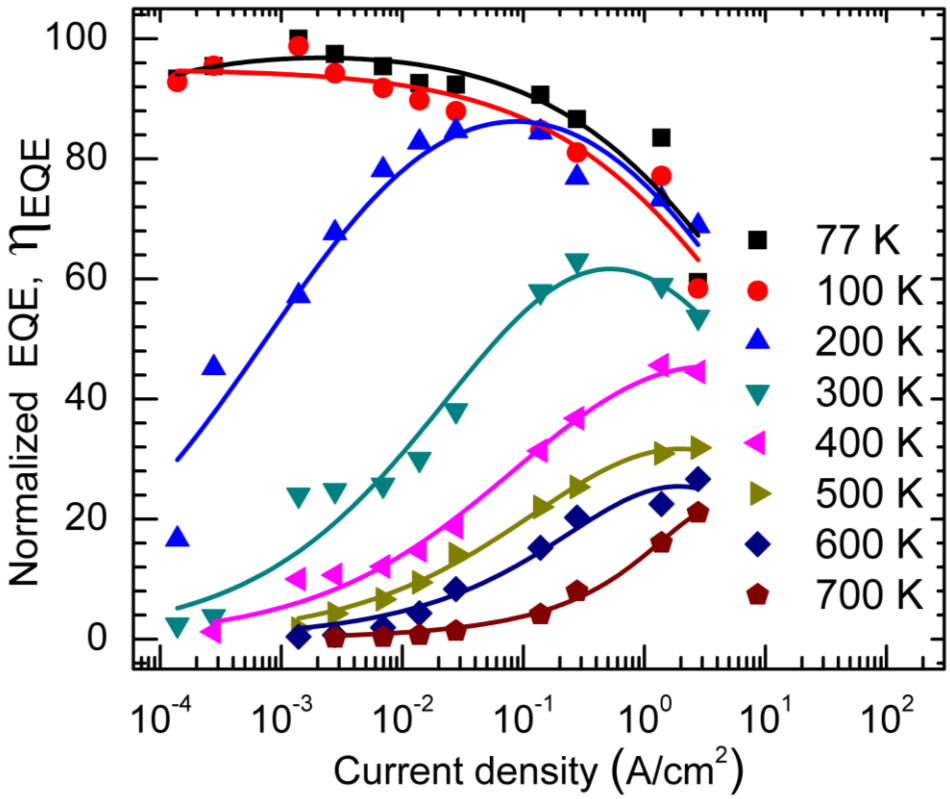

Figure 3.6. Normalized EQE as a function of current density for different temperatures. The dots are the experimental results, solid lines are the fittings of Eq. (6) to the data.

temperatures. The dots are the experimental results, while the solid lines are the fits to Eq. (6). The EQE shows a dome-like shape, similar to the IQE in Fig. 5. The current density at which the peak EQE is observed increases as the temperature rises, which is in agreement with the IQE calculation. Also, the higher injected current levels, the lower the EQE variation with temperature. The EQE evolution slightly differs from IQE, which can be attributed to the change in light extraction efficiency due to the broader temperature range selected.

3.5. Conclusion

The temperature and injected current dependent IQE of the commercial InGaN/GaN MQW blue LED are studied for temperatures up to 700 K. The EL peak energy exhibits a weak S-shaped behavior over the temperature range 77 – 700 K due to carrier localization. The pronounced

phonon replicas at lower temperatures were merged to the main band-to-band transitions at higher temperatures. The sample exhibits a peak IQE of 58.50% at 700 K when it operates at a current density of 2 A/cm^2. It is also noted that the variation in IQE and EQE with temperature is reduced at higher injection current densities. While a higher injection current can cause the LED to fail due to self-heating, an optimized injection level for the LEDs to achieve minimum variation in IQE with temperature can be calculated using the presented method.

References

[1] Sabbar, S. Madhusoodhanan, S. Al-Kabi, B. Dong, J. Wang, S. Atcitty, R. Kaplar, D. Ding, A. Mantooth, S.-Q. Yu, and Z. Chen, "Systematic Investigation of Spontaneous Emission Quantum Efficiency Drop up to 800K for Future Power Electronics Applications," IEEE Journal of Emerging and Selected Topics in Power Electronics, pp. 1–1, 2018.

[2] A. Salhi, M. Alanzi, and B. Alonazi, "Effect of the Quantum-Well Shape on the Performance of InGaN-Based Light-Emitting Diodes Emitting in the 400–500-nm Range," Journal of Display Technology, vol. 11, no. 3, pp. 217–222, 2015.

[3] M. Koike, N. Shibata, H. Kato, and Y. Takahashi, "Development of high efficiency GaN-based multiquantum-well light-emitting diodes and their applications," IEEE Journal of Selected Topics in Quantum Electronics, vol. 8, no. 2, pp. 271–277, 2002.

[4] M. Huang and T. Lu, "Optimization of the Active-Layer Structure for the Deep-UV AlGaN Light-Emitting Diodes," IEEE Journal of Quantum Electronics, vol. 42, no. 8, pp. 820–826, 2006.

[5] Nakamura, S., Akaski, I., Amano, H., In: Pankove J. I., Moustakas T. D., editors. Gallium Nitride I. Academic Press; 1998.

[6] Fong, W., Zhu, C., Leung, B., Surya, C., Sundaravel, B., Luo, E., Wilson, I. (2002). Characterizations of GaN Films Grown with Indium Surfactant by RF-Plasma Assisted Molecular Beam Epitaxy. Microelectronics Reliability, 42(8), 1179-1184. doi:10.1016/s0026-2714(02)00086-0

[7] Li, Z., Waldron, J., Chowdhury, S., Zhao, L., Detchprohm, T., Wetzel, C., Chow, T. P. (2015). High Temperature Characteristics of Monolithically Integrated LED and MOS-

Channel HEMT in GaN Using Selective Epi Removal. Physica Status Solidi (a), 212(5), 1110-1115. doi:10.1002/pssa.201431660

[8] M. Meneghini, L. Trevisanello, G. Meneghesso and E. Zanoni, "A Review on the Reliability of GaN-Based LEDs," in IEEE Transactions on Device and Materials Reliability, vol. 8, no. 2, pp. 323-331, June 2008. doi: 10.1109/TDMR.2008.921527

[9] M. Meneghini, L.-R. Trevisanello, U. Zehnder, T. Zahner, U. Strauss, G. Meneghesso, and E. Zanoni, "High-Temperature Degradation of GaN LEDs Related to Passivation," IEEE Transactions on Electron Devices, vol. 53, no. 12, pp. 2981–2987, 2006.

[10] Peter, M., Laubsch, A., Bergbauer, W., Meyer, T., Sabathil, M., Baur, J., & Hahn, B. (2009). New Developments in Green LEDs. Physica Status Solidi (a), 206(6), 1125-1129. doi:10.1002/pssa.200880926

[11] Wang, J., Johnson, S. R., Ding, D., Yu, S., & Zhang, Y. (2006). Influence of Photon Recycling on Semiconductor Luminescence Refrigeration. Journal of Applied Physics, 100(4), 043502. doi:10.1063/1.2219323

[12] K. Sakowski, L. Marcinkowski, S. Krukowski, S. Grzanka, and E. Litwin-Staszewska, "Simulation of trap-assisted tunneling effect on characteristics of gallium nitride diodes," Appl. Phys. Lett., vol. 111, no. 12, pp. 123115, June, 2012.

[13] Cho, Y., Gainer, G. H., Fischer, A. J., Song, J. J., Keller, S., Mishra, U. K., & Denbaars, S. P. (1998). "S-Shaped" Temperature-Dependent Emission Shift and Carrier Dynamics in InGaN/GaN Multiple Quantum Wells. Applied Physics Letters, 73(10), 1370-1372. doi:10.1063/1.122164

[14] Wang, H., Ji, Z., Qu, S., Wang, G., Jiang, Y., Liu, B., Mino, H. (2012). Influence of Excitation Power and Temperature on Photoluminescence in InGaN/GaN Multiple Quantum Wells. Optics Express, 20(4), 3932. doi:10.1364/oe.20.003932

[15] Fan, S., Villeneuve, P., & Joannopoulos, J. (2000). Rate-Equation Analysis of Output Efficiency and Modulation Rate of Photonic-Crystal Light-Emitting Diodes. IEEE Journal of Quantum Electronics, 36(10), 1123-1130. doi:10.1109/3.880652

[16] Meyaard, D. S., Shan, Q., Cho, J., Schubert, E. F., Han, S., Kim, M., Kim, J. K. (2012). Temperature Dependent Efficiency Droop in GaInN Light-Emitting Diodes with Different Current Densities. Applied Physics Letters, 100(8), 081106. doi:10.1063/1.3688041

4. High-Temperature Optical Characterization of GaN-Based LEDs for Future Power Electronic Modules

4.1. Abstract

High-temperature optical analysis of three different InGaN/GaN MQW LED structures (peak wavelength λp = 448nm, 467 nm & 515nm) is conducted for possible integration as an optocoupler emitter in high-density power electronic modules. The commercially available LEDs, primarily used in the display (λp = 467 nm & 515nm) and lighting (λp = 448nm) applications, are studied and compared to evaluate if they can satisfy the light output requirements in the optocouplers at high temperatures. The temperature- and intensity-dependent electroluminescence (T-IDEL) measurement technique is used to study the internal quantum efficiency (IQE) of the LEDs. All three LEDs exhibits above 70 % IQE at 500 K, and stable operation at 800 K without flickering or failure. At 800 K, a promising IQE of above 40 % is observed for blue for display (λp = 467 nm) and green for display (λp = 515nm) samples. Blue for light (λp = 448nm) sample shows 24 % IQE at 800 K.

4.2. Introduction

The rigorous research in silicon carbide (SiC) technology drives the fast-paced development of power electronics in recent years. Silicon carbide technology enables high-temperature operation of power modules with higher power density and faster-switching speeds compared with the conventional silicon power modules [1]. Reliable high-temperature operation of SiC-based power devices helps develop power modules suitable for size- and weight-sensitive applications such as electric vehicles, motor drives, and space exploration by eliminating the extensive cooling system associated with the power module. The overall size of the power

electronics module is now decided by passive components such as bulky transformers. Typically, multiple transformers with large form-factor are used as the galvanic isolation system in power modules to float the high voltage gate driver. The modulation and demodulation circuits associated with the isolation transformers add to the complexity of gate driver design. Therefore, using isolation transformers of high form-factor limits scaling-down of power electronic modules [2]. A further scale down of power modules is possible by replacing bulky transformers with optocouplers of low form-factors. However, the low performance of optoelectronic devices due to the degradation of quantum well efficiency, metallization, and packaging at high temperatures and operating conditions prevents the use of optocouplers in high-density power modules [3]. A systematic study of the high-temperature operation of optoelectronic devices, i.e., emitters and photodiodes, is necessary to overcome the limiting factors in developing the high-temperature optocouplers. Thus far, a minimal reported study is available in the literature on the high-temperature application of optoelectronic devices [4].

The high-efficiency and high-brightness GaN-based light-emitting diodes (LEDs) are promising candidates for high-temperature operation due to their unique properties, such as wide bandgap, low heat dissipation, and higher operating lifetime compared to gallium arsenide (GaAs) or gallium phosphide (GaP) based LEDs [5]. Therefore, a systematic investigation of the performance of GaN-based LEDs at high temperatures helps examine the possibility of optical integration on SiC-based high-density power modules. A previous study conducted on InGaN/GaN multiple quantum well (MQW) green optoelectronic material with a peak wavelength of 516 at room temperature reports that the internal quantum efficiency (IQE) of above 44 % is achievable at 527 ^{o}C [4]. The reported IQE of 44 % is acceptable for high-temperature optocoupler emitter application as long as the photodetector is not degraded in the optocoupler.

The IQE of LEDs at a given temperature is a function of injected current density. A non-optimal selection of injection current density can cause a higher drop in IQE at elevated temperatures. Though the previous study on the LED epitaxy material confirms the reliable high-temperature operation, a systematic study of the LED devices is needed in designing optimal biasing conditions. Besides the biasing conditions, the high-temperature operation of the LED devices is also affected by the device geometry, contact metallization, and packaging [6]. The selection of contact metallization and packaging for high-temperature applications is studied in detail in the past [7]. The effect of quantum well (QW) structure on designing emitters for high-temperature applications needs to be understood.

In this paper, a comparative study is conducted on the IQE of commercial InGaN/GaN MQW LEDs with different QW structures. Bare die LEDs are selected in order to avoid high-temperature optical degradation due to packaging materials. Traditional ABC model is used to extract the IQE as a function of injected current density. The focus of the study is to evaluate the possibility of operating InGaN/GaN MQW LEDs at high temperatures and to determine the optimal current density to achieve peak IQE at different temperatures.

4.3. Experimental section

High-temperature measurements on the LED devices were carried out in a Janis ST-100 cryostat, and the electroluminescence (EL) spectra were collected using a Horiba 550 spectrometer integrated with a photomultiplier tube (PMT). During all measurements, the self-heating of the LED devices with a turn-on voltage of under 2.0 V was avoided by limiting the current density to 0.25 A/cm^2 and 1.0 A/cm^2 for light and display samples, respectively. The device structure and IQE extraction methods using ABC modeling are explained in detail in the following sections.

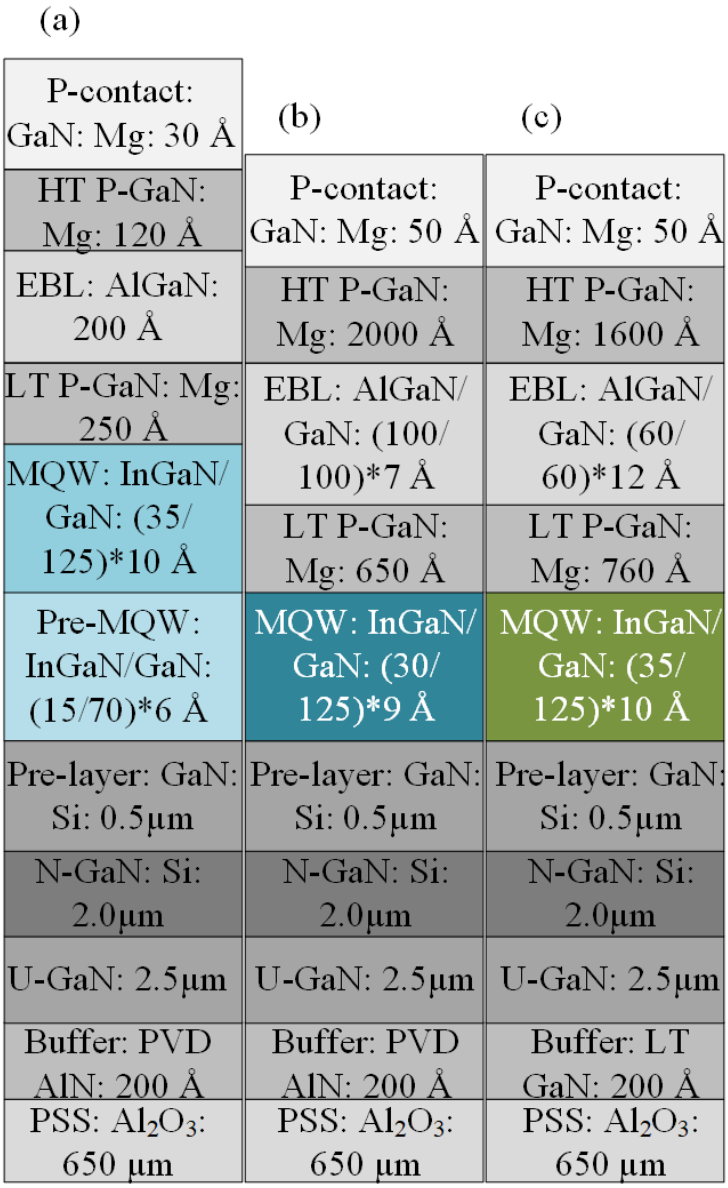

Figure 4.3 Schematic of the epitaxial structure of (a) blue for light (b) blue for display and (c) green for display LEDs.

The InGaN/GaN MQW LEDs, grown on patterned sapphire substrates, were supplied by HC SemiTek. Figure 4.1 shows the detailed schematic structure of the three LEDs with a peak emission wavelength of 454 nm, 472 nm & 523 nm at room temperature, which are named blue for light (BL), blue for display (BD) and green for display (GD), respectively. Blue LED samples, i.e., BL and BD, consists of a 20 nm aluminum nitride (AlN) buffer layer, whereas the GD sample

has a 20 nm GaN as a buffer layer. The active regions studied consists of ten 3.5 nm InGaN QWs with 12.5 nm GaN barrier layers for the BL and GD samples, whereas the BD sample consists of nine 3.0 nm InGaN QWs with 12.5 nm GaN barrier layers. A pre-MQW layer consisting of six 1.5 nm undoped InGaN QWs with 7 nm Si-doped GaN barriers is also included in the BL LED structure. The display LEDs, BD and GD, consists of seven and twelve periods of AlGaN/GaN superlattice electron blocking layers (EBL) before the magnesium-dopped p-GaN layer and the p++-GaN contact layer. The BL LED structure includes a 20 nm bulk AlGaN EBL before the magnesium-dopped p-GaN layer and the p++-GaN contact layer.

IQE Modelling:

To extract the IQE of LEDs using ABC modeling, temperature- and injected current-dependent electroluminescence (T-IDEL) measurements were conducted. The ABC model provides excellent fitting of quantum efficiency measured in a wide range of operating currents. In order to identify the peak IQE and optimum injected current density, a modeling technique is more suitable rather than the traditional room temperature-low temperature PL/EL comparison. The measured EL intensities for different temperatures and injected current densities were fitted using the power-law relationship. Power law states that the electron-hole pair photoexcitation density is proportional to the current injection density, J_{EL}. Also, the spontaneous emission rate per unit area per unit length from the active region is proportional to the EL signal integrated over energy, L_{EL}. The relationships are described by:

$$J_{EL} = \frac{c_a}{\eta_{inj}}[An + (1-\gamma_r)Bn^2 + Cn^3]\ ;\ L_{EL} = c_b\eta_{ext}Bn^2 \qquad (1)$$

where ca and cb are constants of proportionality determined by sample and measurement geometry. The current injection efficiency and the light extraction efficiency of the LED are denoted by ηinj and ηext, respectively. For this study, the photon recycling factor, γr, is assumed

to be zero [8]. The recombination coefficients for the Shockley-Reed-Hall (SRH), radiative, and Auger mechanisms are denoted by A, B, and C, respectively. Recombination rates are presented as the powers of electron-hole concentration n.

The injection current density J_{EL} can be expressed as a function of L_{EL} from Equation 1 as follows:

$$J_{EL} = A_{EL}{L_{EL}}^{1/2} + B_{EL}L_{EL} + C_{EL}{L_{EL}}^{3/2} \quad (2)$$

where A_{EL}, B_{EL}, and C_{EL} are the best-fit parameters calculated by fitting Equation 2 to the experimental data, as shown in Figure 4.2.

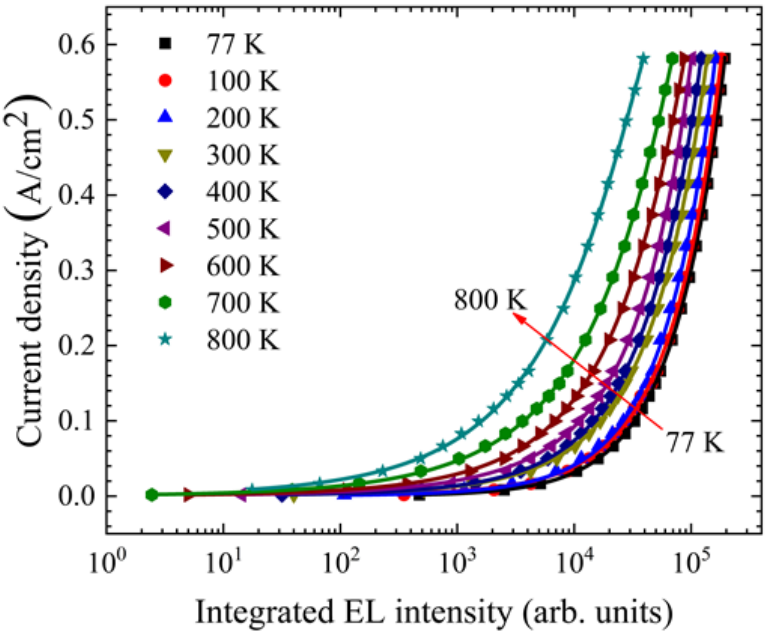

Figure 4.2. Integrated EL intensity as a function of current density is plotted for different temperatures. The dots are the experimental results, solid lines are ABC fittings to the data for blue for display sample.

The internal quantum efficiency of the LED is defined as:

$$\eta_{IQE} = \frac{Bn^2}{An + Bn^2 + Cn^3} \quad (3)$$

Using Equation 1 and 2, internal quantum efficiency can be expressed as:

$$\eta_{IQE} = \left(1 + \frac{A_{EL}}{B_{EL}}\left(\frac{1}{\sqrt{L_{EL}}}\right) + \frac{C_{EL}}{B_{EL}}\sqrt{L_{EL}}\right)^{-1} \quad (4)$$

4.4. Results and Discussion

Temperature-dependent EL spectra of BL, BD, and GD samples at an injected current density of 0.25A/cm^2 are shown in Figure 4.3. The inset of the figures shows the evolution of peak wavelength over the temperature. A drop in EL intensity and spectral broadening is observed in all the samples at high temperatures. Blue for light sample shows pronounced phonon replicas at low temperatures, which merged to band-to-band transitions at higher temperatures.[9] The phonon-replicas in the display samples are not prominent due to the comparatively low nominal indium content. A higher nominal indium content enhances the momentum transfer from the defects, which indeed created by the prominent indium aggregation and phase separation, in meeting the requirement of momentum conservation in the phonon–replica transition. All the three samples exhibit an S-shaped EL peak energy evolution over the temperature range, which is typically attributed to carrier localization [10]. To quantitatively study the thermal droop, EL spectra are integrated over the energy and plotted for different temperatures. Figure 4.4 shows the normalized integrated EL intensity of BL, BD, and GD samples at an injected current density of 0.25A/cm^2 for different temperatures. A targeted operating temperature range is defined from 300 – 500 K in accordance with the development of high-temperature optocoupler. A three order of magnitude reduction in EL intensity is observed from the BL sample whereas the display samples show one order magnitude reduction in EL intensity. Three order magnitude reduction in EL intensity points to a significant drop in IQE at higher temperatures. However, the thermal droop, i.e., drop in LED efficiency at higher temperatures, is dependent on the injected current density. A

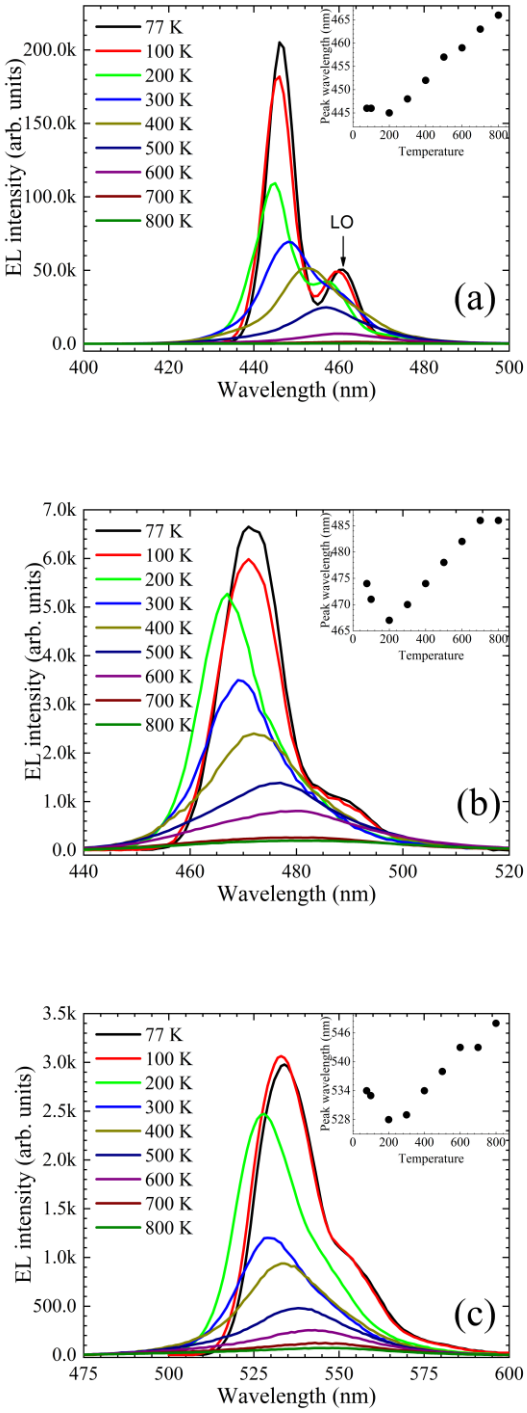

Figure 4.4. EL spectra of (a) blue for light (b) blue for display and (c) green for display LEDs measured at a injected current density of 0.25A/cm2 for different temperatures. Inset shows the evolution of EL peak position with temperature.

different injected current can alter the behavior of the LED light intensity drop at elevated

temperatures. Therefore, the reduction in LED light intensity at elevated temperatures can be minimized by the optimal selection of injected current density.

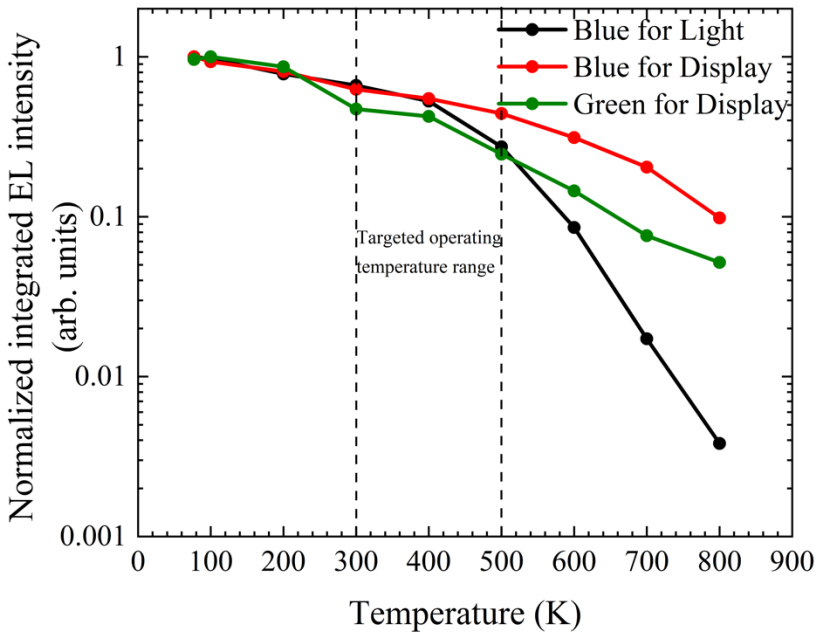

Figure 4.4. Normalized integrated EL intensity of BL, BD, and GD LEDs is calculated from the respective EL spectra at an injected current density of 0.25 A/cm^2 and plotted as a function of temperature.

The IQE of LEDs as a function of injected current density is extracted for different temperatures using the ABC model. Figure 4.5 shows the evolution of IQE at elevated temperatures for light and display samples. The dots are the experimental points and the solid lines are fits of Equation 4. Equation 2 is used to accommodate injected current densities as a function of IQE. The IQE of LED structures shows a dome-like structure with peak IQE at different temperatures occurring at different injected current densities. It is also observed that the width of the dome-like structure decreases at elevated temperatures resulting in a lower peak IQE value. The IQE of all three LEDs tends to merge at high injected current densities. The IQE increases

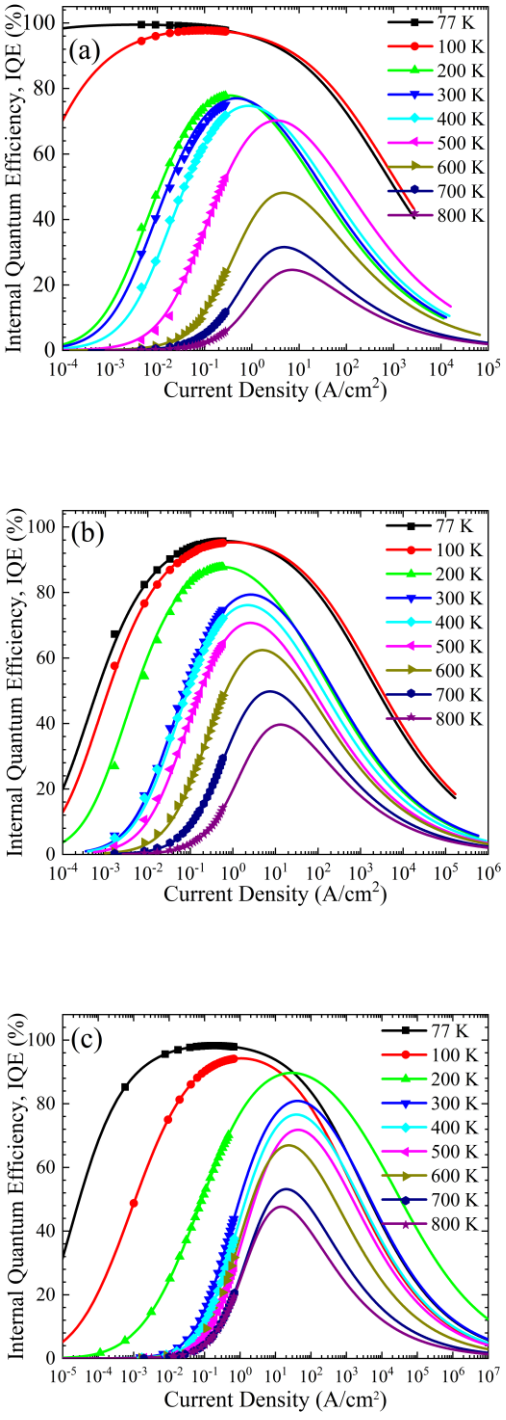

Figure 4.5. Internal quantum efficiency is plotted as a function of current density at different temperatures for (a) blue for light (b) blue for display and (c) green for display LEDs.

with the increase in injected current density until it reaches the peak value and starts to degrade. The drop in IQE at higher injected current densities, i.e., current droop, is commonly attributed to the enhanced Auger recombination at increased current density [11]. Although the drop in current injection efficiency also contributes to the current droop, the enhanced Auger recombination dominates at higher injected current densities.

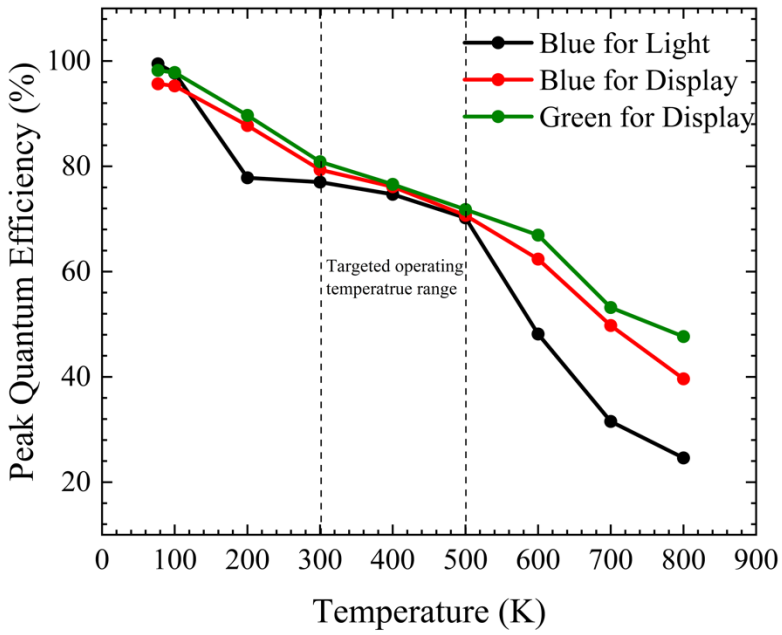

Figure 4.6. The peak IQE of BL, BD and GD LEDs at different temperatures are extracted and plotted as a function of temperature.

The evolution of Peak IQE as a function of temperature for light and display LEDs is shown in Figure 4.6. All three LEDs show three different slopes in the peak IQE curve over the temperature range from 77 - 800 K. At low-temperature range (77 -300 K), the peak IQE tends to decrease when the temperature increases. In the targeted operating temperature range, LEDs show a stable IQE with less than 10 % reduction in the peak IQE. The extracted peak IQE for BL, BD,

and GD at 500 K are 70, 71 and 72 % respectively. Increasing the temperature above 500 K causes a significant drop in peak IQE. At 800 K, the BL, BD and GD samples show peak IQE of 24, 40 and 48 % respectively. It is observed that the GD LED shows the highest peak IQE from 100 – 800 K, followed by BD and BL LEDs. A systematic analysis based on the LED structure is needed to conclude the peak IQE behavior of the LEDs. However, it is difficult in this study as there is more than one parameter change across LED structures as shown in Figure 4.1. A pre-MQW layer in the LED structure improves the efficiency of InGaN based LEDs [12]. However, the peak IQE

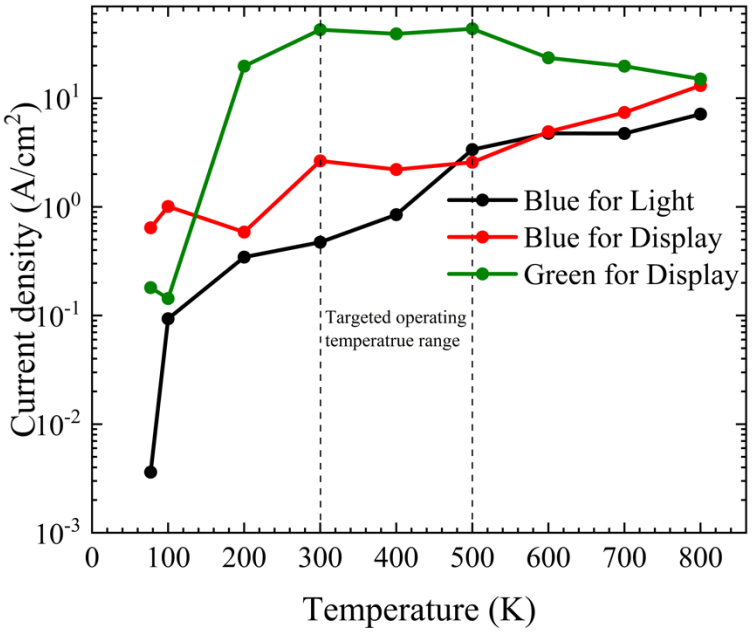

Figure 4.7. The current injection density corresponding to the peak IQE, jp_{IQE}, of BL, BD and GD LEDs at different temperatures are extracted and plotted as a function of temperature.

of BL LED with a pre-MQW layer and a higher number of QWs in the active region shows lower peak IQE than the LED structures without the pre-MQW layer. The higher peak IQE of the BD and GD LEDs can be attributed to the presence of GaN buffer layer and superlattice EBL. Studies show that using an LT GaN buffer layer instead of the AlN buffer layer improves the crystal quality and leads to higher IQE [13]. Also, replacing the conventional bulk EBL with a superlattice

structure can enhance the efficiency and reduce the droop in LEDs.[14] Although the GD LED shows a higher peak IQE at elevated temperatures, it is observed that the injected current density to achieve peak IQE, jp_{IQE}, is higher than other LEDs. The change in jp_{IQE} over the temperature range is shown in Figure 4.7. In the targeted operating temperature range, the jp_{IQE} of GD LED is one order of magnitude higher than that of BD. A higher jp_{IQE} of GD sample can be attributed to the superlattice structure of the EBL. However, high injected current levels can shorten the lifetime of LED devices. To develop the high-temperature LEDs for continuous operation at 250oC, the trade-off between the IQE and injected current density needs to be understood. A stable peak IQE and a lower jp_{IQE} is therefore suitable for the continuous operation of LEDs at elevated temperatures.

4.5. Conclusion

The temperature and injected current dependent IQE of commercial InGaN/GaN MQW LEDs with different QW structures are studied over the temperature range from 77 - 800 K. The peak IQE of LED samples at different temperatures and the respective injected current density is extracted using ABC model. The structural difference across the LED samples has a pronounced effect on the IQE drop at higher temperatures. The GD sample exhibits the highest peak IQE in the temperature range 100 -800 K followed by BD and BL. The presence of pre-MQW layer has little effect on improving the peak IQE of LED devices as compared to the presence of LT GaN buffer layer and the superlattice EBL structure. A superlattice EBL in the LED structure tends to increase the jp_{IQE} of the sample as compared to conventional bulk EBL. A stable peak IQE and a lower jp_{IQE} across the targeted temperature range are suitable options for the selection of LEDs to integrate into high-temperature optocouplers.

References

[1] R. Maboudian, C. Carraro, D. G. Senesky, and C. S. Roper, “Advances in silicon carbide science and technology at the micro- and nanoscales,” Journal of Vacuum Science & Technology A: Vacuum, Surfaces, and Films, vol. 31, no. 5, p. 050805, 2013.

[2] B. Rowden, A. Mantooth, S. Ang, A. Lostetter, J. Hornberger, B. McPherson, “High Temperature SiC Power Modules,” ASME 2009 In-ternational Mechanical Engineering Congress & Exposition (IMECE), 2009.

[3] F. Huang, L. Yin, S. Li, G. Xu, H. Yan, Y. Chen, L. Yang, and J. Zhang, “Study on the reliability of high-power LEDs under temperature cycle,” 2011 12th International Conference on Electronic Packaging Technology and High Density Packaging, 2011.

[4] S. Nakamura and M. R. Krames, “History of Gallium–Nitride-Based Light-Emitting Diodes for Illumination,” Proceedings of the IEEE, vol. 101, no. 10, pp. 2211–2220, 2013.

[5] A. Sabbar, S. Madhusoodhanan, S. Al-Kabi, B. Dong, J. Wang, S. Atcitty, R. Kaplar, D. Ding, A. Mantooth, S.-Q. Yu, and Z. Chen, “Systematic Investigation of Spontaneous Emission Quantum Efficiency Drop up to 800K for Future Power Electronics Applications,” IEEE Journal of Emerging and Selected Topics in Power Electronics, pp. 1–1, 2018.

[6] M. Koike, N. Shibata, H. Kato, and Y. Takahashi, “Development of high efficiency GaN-based multiquantum-well light-emitting diodes and their applications,” IEEE Journal of Selected Topics in Quantum Electronics, vol. 8, no. 2, pp. 271–277, 2002.

[7] R. Zeiser, P. Wagner, and J. Wilde, “Assembly and packaging technologies for high-temperature SiC sensors,” 2012 IEEE 62nd Electronic Components and Technology Conference, 2012.

[8] Wang, J., Johnson, S. R., Ding, D., Yu, S., & Zhang, Y. (2006). Influence of Photon Recycling on Semiconductor Luminescence Refrigeration. Journal of Applied Physics, 100(4), 043502. doi:10.1063/1.2219323.

[9] Y.-H. Cho, G. H. Gainer, A. J. Fischer, J. J. Song, S. Keller, U. K. Mishra, and S. P. Denbaars, “‘S-shaped’ temperature-dependent emission shift and carrier dynamics in InGaN/GaN multiple quantum wells,” Applied Physics Letters, vol. 73, no. 10, pp. 1370–1372, 1998.

[10] C. H. Wang, S. P. Chang, W. T. Chang, J. C. Li, H. C. Kuo, T. C. Lu, and S. C. Wang, “Efficiency droop improvement in GaN-based light emitting diodes by graded-composition electron blocking layer,” Eleventh International Conference on Solid State Lighting, 2011.

[11] P. Törmä, O. Svensk, M. Ali, S. Suihkonen, M. Sopanen, M. Odnoblyudov, and V. Bougrov, “Effect of InGaN underneath layer on MOVPE-grown InGaN/GaN blue LEDs,” Journal of Crystal Growth, vol. 310, no. 23, pp. 5162–5165, 2008.

[12] M. Benamara, Z. Liliental-Weber, J. Mazur, W. Swider, J. Washburn, M. Iwaya, I. Akasaki, and H. Amano, “The Role of the Multi Buffer Layer Technique on the Structural Quality of GaN,” MRS Internet Journal of Nitride Semiconductor Research, vol. 5, no. S1, pp. 398–404, 2000.

[13] J. Tong and S. Li, “Droop Improvement in Blue InGaN Light Emitting Diodes with AlGaN/InGaN Superlattice Barriers,” Asia Communications and Photonics Conference, 2012.

5. High-Temperature Analysis of GaN-based MQW Photodetector for Optical Galvanic Isolations in High-Density Integrated Power Modules

5.1. Abstract

The InGaN/GaN MQW structure is demonstrated as a possible solution for high-temperature photodiode applications. High temperature spectral and noise analysis of InGaN/GaN MQW structure are performed for the potential integration as a detector in future power electronics applications. The spectral response was measured under photovoltaic and bias modes for the temperature range of 77 - 800 K. A peak spectral responsivity of 27.0 mA/W at 440 nm at 500 K is recorded. The peak external quantum efficiency of the device was calculated to be in the range of 5 - 8 % in the temperature range 77 - 800 K. The photodetector sensitivity of the structure is quantified using the material figure of merit parameter, D* for different temperature and biased voltages. A peak detectivity of 4 x 108 $cmHz^{1/2}W^{-1}$ is observed at 800 K with zero bias at 440 nm.

5.2. Introduction

The necessity of high-temperature power electronics for applications such as aeronautics, hybrid automotive, space exploration, and deep oil-gas exploration has reformed the research focus from ubiquitous silicon (Si) to wide bandgap (WBG) materials such as silicon carbide (SiC) and gallium nitride (GaN) [1-3]. When compared to the Si-based power devices, the higher performance of SiC devices in terms of operation temperature, output power, controllability, and higher switching speeds makes them more attractive in high power and extreme temperature applications. Implementing SiC technology in high-temperature power modules helps lower the system form factor by eliminating bulky cooling systems and incorporating smaller passive elements. The high scalability of SiC power modules attracts various size and weight-sensitive

applications such as electric vehicles and space shuttles in the past decades. To thoroughly exploit the high-temperature capability of SiC power devices and achieve high scalability, researchers focused on the integration of the gate drive with SiC power module that requires a high-temperature operation of gate drive circuitry [4]. However, further scaling of power modules is now limited by passive components such as isolation transformers. A galvanic isolation circuitry prevents noise propagation and guarantees the robustness of the power module. The gate drive signals could use magnetic or capacitive isolation [5,6]. Bulky isolation transformers are often replaced with comparatively low form factor optocouplers in gate drive control circuitry that operates at a relatively low temperature compared to the power module. However, the integrated power modules cannot use optocouplers due to the efficiency drop of optical devices and the high-temperature packaging requirements. Therefore, a systematic study is required to develop high-temperature optocouplers to use in high-density integrated power modules.

The development of high-temperature optocouplers involves a systematic approach to develop emitters, detectors, packaging, and dielectric materials. We previously reported several studies to evaluate the feasibility of commercial LEDs as the emitters in high-temperature optocoupler [7-9]. The reported studies reveal that GaN-based multiple quantum well (MQW) LEDs exhibit stable operation at the targeted operating temperature at 250 ^{o}C. These promising results lead to the study of different detectors suitable for high-temperature operation. The initial study comprises of the high-temperature spectral characterization of different commercially available detectors. Figure 5.1 shows a comparison in the temperature-dependent spectral response of bare-die Si, SiC, and InGaN based photodiodes. The spectral response of the detectors is normalized at 300 K. Si-based photodetectors are widely used in the optoelectronics field due to its wide detection range and higher responsivity. However, Si-based photodetectors are not

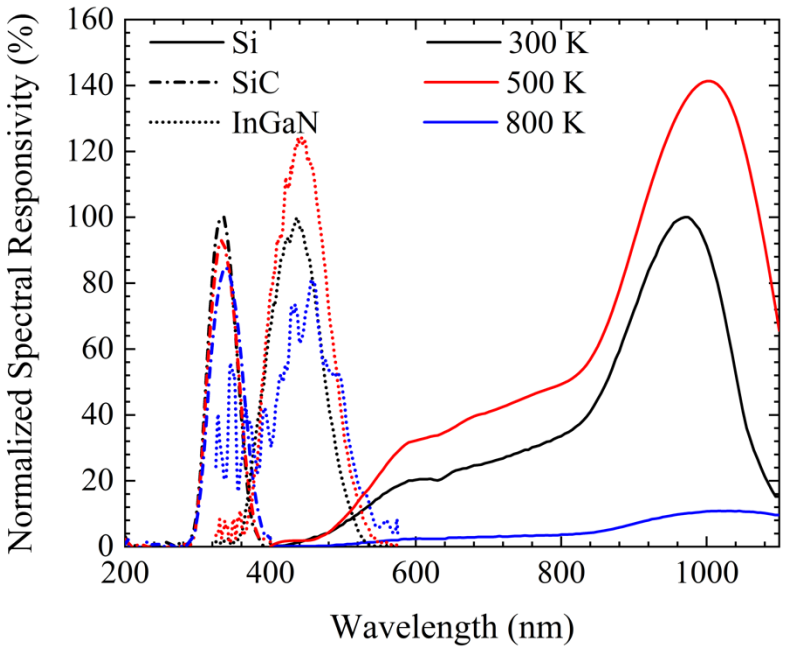

Figure 5.1. Temperature dependent spectral response of Si, SiC and InGaN based photodiodes.

suitable candidates for high-temperature operation. The responsivity of Si-based photodiodes degrades rapidly at elevated temperatures starting from 150 ^{o}C. Photodiodes based on SiC are widely proposed in the literature in the last decade for application requiring high-temperature operation, chemical inertness, and radiation hardness [10-12]. Stable high-temperature operation of SiC photodiodes based both on Schottky and p-i-n junction are reported in the literature [13-15]. The typical wavelength range of SiC photodiodes varies from 200 nm to 400 nm [10-16]. However, a suitable emitter in the UV range with the stable high-temperature operation, higher intensity, and compatible with optocoupler design is not reported anywhere.

In recent years, researchers focused on developing GaN-based photodetectors for visible and near-ultraviolet ranges. High-temperature operation and tolerance to radiation damages of GaN-based detectors make them more attractive to space exploration and combustion applications. However, various studies indicate that using bulk indium gallium nitride (InGaN) layers leads to

issues such as non-abrupt absorption edges and poor detection contrasts [17-19]. As the indium (In) concentration in the layer increases, the issues get worsened due to the increase in alloy segregation and clustering. These technical issues can be suppressed by using GaN-based MQW structures. It is also reported that the device performance improves in the MQW structure due to low photodetector dark current and the presence of internal gain mechanism [20].

In this paper, we report a systematic study on the photodetector performance of the InGaN/GaN MQW LED bare-die devices with a wide range of temperatures from 77 – 800 K. The rationale for selecting the GaN-based MQW structure can be explained by i) stable high-temperature operation and to suppress the previously reported alloy segregation and clustering issue of bulk InGaN layers ii) to achieve better coupling efficiency with the previously reported LEDs [7-9]. The experiments were performed on bare-die devices to eliminate any unwanted degradation due to packaging materials. Temperature-dependent spectral response analysis was performed under photovoltaic and biased modes. The specific detectivity of the device was extracted at temperatures up to 800 K. This study demonstrates the feasibility of the InGaN/GaN MQW structure as a possible solution for the high-temperature photodiodes in future power electronic applications.

5.3. Experiment

Figure 5.2 shows the detailed schematic structure of the InGaN/GaN MQW LED structure grown on patterned sapphire substrates (PSS) with a 20 nm GaN as a buffer layer. The active region studied consists of ten 3.5 nm InGaN QWs with 12.5 nm GaN barrier layers. The sample consists of twelve periods of AlGaN/GaN superlattice electron blocking layers (EBL) before the magnesium-doped p-GaN layer and the p++-GaN contact layer. The MQW structure

exhibits an electroluminescence peak at 535 nm at 300 K. A detailed description of the growth parameters of the InGaN/GaN MQW LED structure used for this study is reported elsewhere [9].

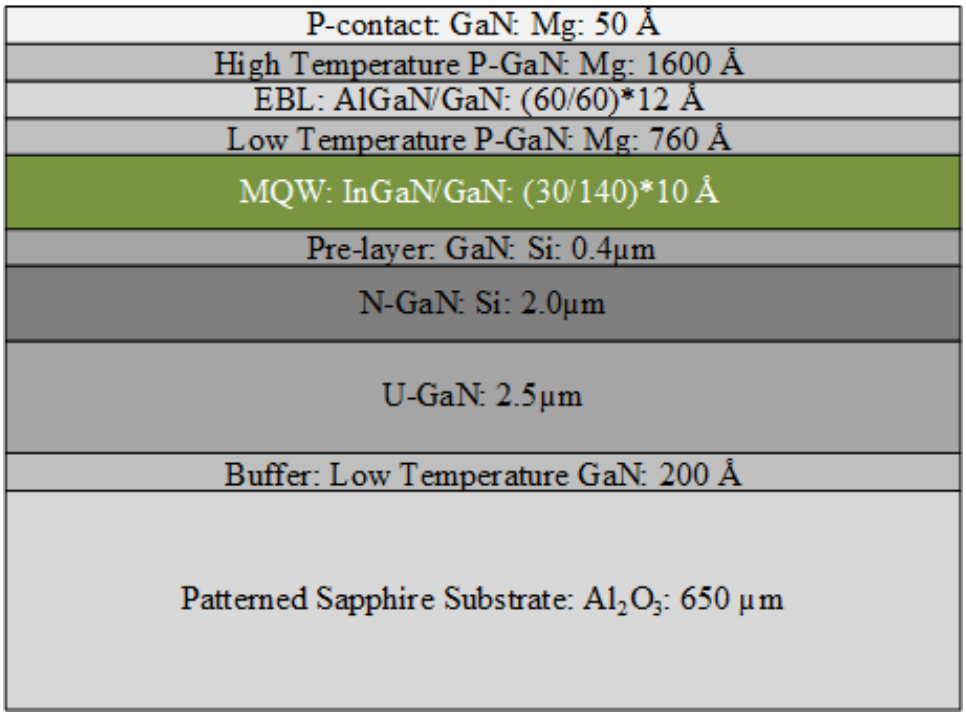

Figure 5.2. Schematic diagram of the InGaN/GaN MQW LED epitaxial structure.

High-temperature characterization of the MQW structure was carried out in a Janis ST-100 cryostat. The spectral responses of the structure were obtained using a tunable monochromator with a 250W, 24V tungsten halogen lamp. A calibrated Si detector is used to measure the incident power on the MQW structure from the monochromator. The photocurrents were measured using a lock-in amplifier based on which the responsivity, $\Re$, is extracted. A Keithley 236 source measurement unit (SMU) was used to measure the dark current-voltage (I-V) characteristics in the temperature range 77 -800 K.

The photodetector sensitivity of the structure is quantified using the material figure of merit parameter D*, calculated in units of Jones (cm $Hz^{1/2}W^{-1}$), as below:

$$D^* = \frac{\sqrt{A\Delta f}}{i_{rms}}\Re \quad (1)$$

where A is the active detecting area of the structure in square centimeter, Δf is referred to the equivalent noise bandwidth (ENBW) in hertz, $\Re$ is the spectral responsivity in ampere per watt, and i_{rms} is the root mean square of noise currents in the detector system. In this study, Δf is taken as 1 Hz. The i_{rms} , which includes Johnson or thermal noise, shot noise, generation-recombination noise, and 1/f noise, is calculated as follow:

$$i_{rms} = \sqrt{i_{thermal}^2 + i_{shot}^2 + i_{G-R}^2 + i_{1/f}^2} \quad (2)$$

The generation-recombination noise occurred due to the random generation, and the recombination of free carriers caused by crystal vibrations is considered as zero in this study as this occurs mainly in photoconductors and is limited by diffusion in an ideal photodiode. Also, 1/f noise or flicker noise is eliminated in this study as the noise level is negligible for detector works under high frequency. The thermal and shot noise is calculated using the following equations:

$$i_{thermal} = \sqrt{4kT\Delta f/R_0} \;\; ; \; i_{shot} = \sqrt{2qI\Delta f} \quad (3)$$

where k is the Boltzmann constant, T is the absolute temperature, R_0 is the resistance of the device, q is the charge of an electron, and I is the average current flow in the device under illumination, which includes both photocurrent and dark current. In this study, noise bandwidth was set by configuring the time constant and slope/oct of the lock-in amplifier to 100 ms and 18 dB/oct, respectively.

The device figure of merit, noise equivalent power (NEP), i.e., the minimum impinging optical power that a detector can distinguish from noise, is calculated as follows:

$$NEP = i_{rms}/\Re \tag{4}$$

Also, the D^* is related to NEP as follows:

$$D^* = \frac{\sqrt{A\Delta f}}{NEP} \tag{5}$$

5.4. Results and Discussion

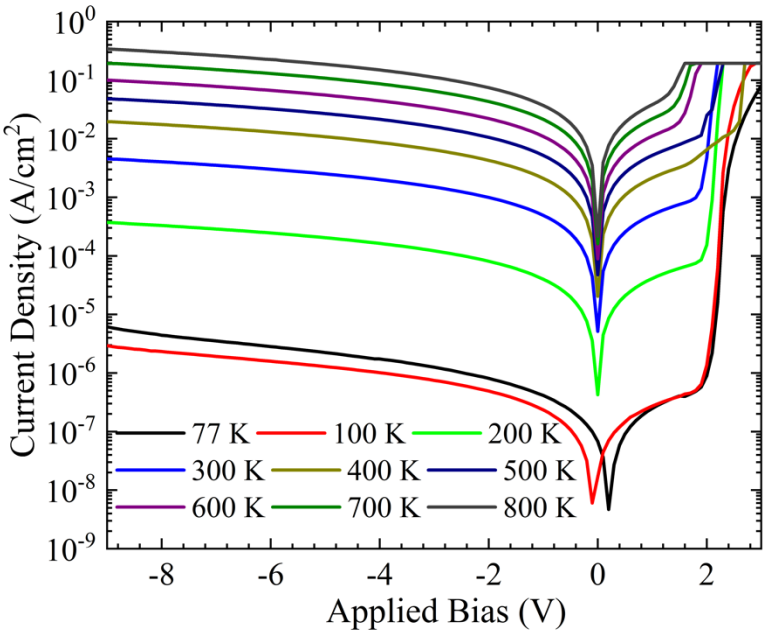

Figure 5.3. I-V characteristics of the InGaN/GaN MQW structure for temperatures from 77 - 800 K.

The dark I-V characteristics of the InGaN/GaN structure for temperatures from 77 -800 K is shown in Fig. 5.3. The dynamic resistances were extracted from the dark I-V characteristics for the accurate calculation of noise levels. Although the measurements were performed under a non-illuminated condition, there is an effect of background low-illumination causing relatively small but finite zero-bias minority carrier current. Therefore, the dynamic resistance extraction was

performed based on the curve fitting process. The leakage current density of the structure increased by five orders of magnitude as the temperature increases from 77 – 800 K. The leakage current is a function of both temperature and applied bias, suggesting a combination of tunneling and thermally generated currents. It is also observed that a rapid increase in the leakage current when

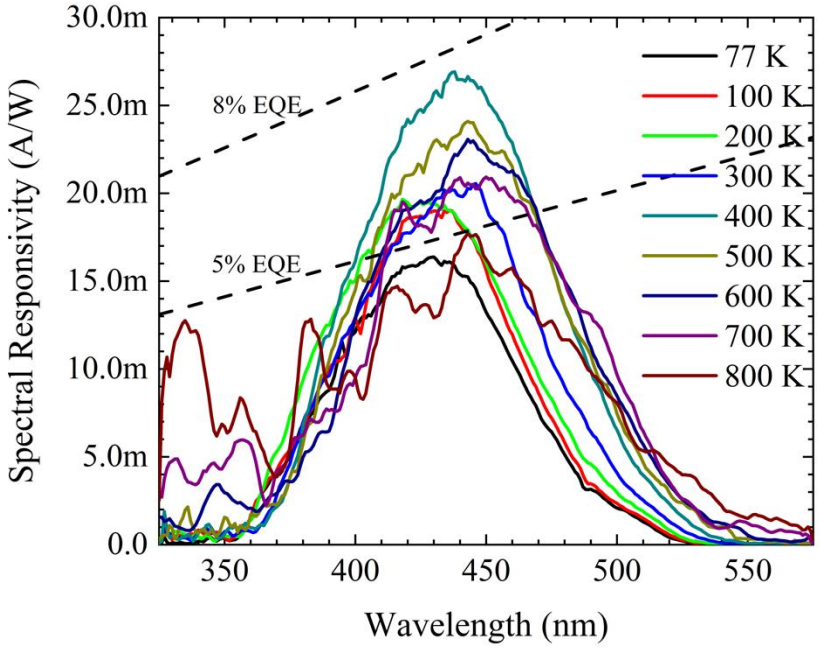

Figure 5.4. Spectral response of the InGaN/GaN MQW structure for different temperatures at zero bias. Dashed lines represent the respective EQE.

the temperature is increased from 100 K to 200 K. This rapid increase in the leakage current can be attributed to thermal ionization of carriers from deep traps and trap assisted tunneling process.

The spectral response of the MQW structure was measured from 77 – 800 K at different biased conditions. Figure 5.4 shows the calculated spectral responsivity of the sample at zero bias voltage. The spectral responsivity peaks at 440 nm, corresponding to the barrier heights, due to the lower absorption depth in the QWs. The number of QWs in the space charge region (SCR) also affects the spectral responsivity from the wells. However, not all the QWs fall into the SCR. A

redshift in the spectral response peak and the detection edge is observed when the temperature increases from 77 K to 500 K. An increase in the peak spectral responsivity is also observed in this temperature range. The sample shows a peak spectral responsivity of 27.0 mA/W at 440 nm at 500 K. Increasing the temperature above 500 K leads to a decrease in the peak spectral responsivity along with the redshift of the spectrum. The redshift of the spectral peak at elevated temperatures is attributed to the bandgap shrinkage. The peak EQE of the device was calculated to be in the

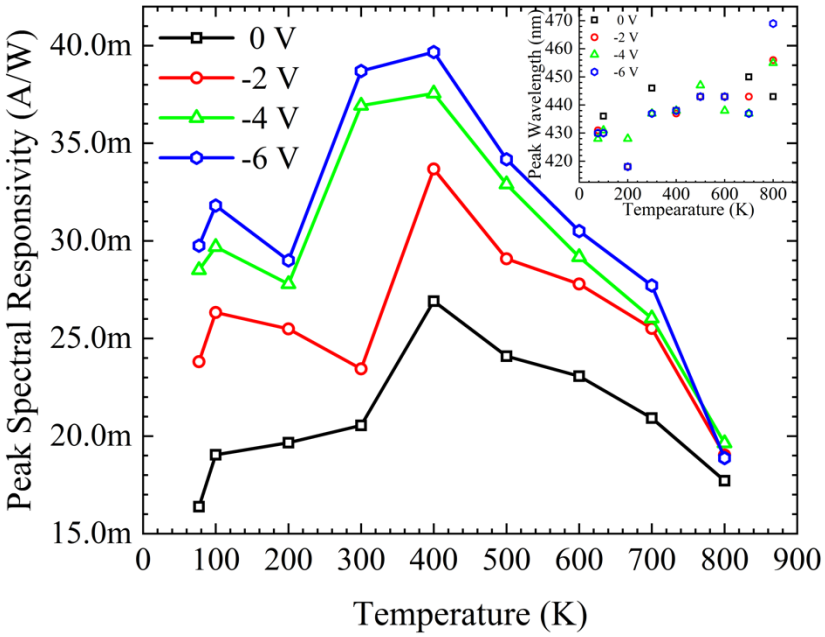

Figure 5.5. Peak spectral response of the InGaN/GaN MQW structure is plotted as a function of temperature for different biased conditions. Inset shows the evolution of wavelength corresponding to the peak spectral response.

range of 5 - 8 % in the temperature range 77 - 800 K.

Figure 5.5 shows the peak spectral responsivity of the sample at different temperatures and biased conditions; inset of the figure shows the respective wavelength. The wavelength corresponding to the peak spectral response shows an S-shaped behavior, confirming the carrier localization effect. The peak spectral responsivity tends to increase when the temperature increases

from 77 K to 400 K at zero bias. The increase in the spectral responsivity with the temperature is ascribed to (i) the enhanced absorption length at longer wavelengths, (ii) reduction in the effective barrier height imposed by the AlGaN/GaN EBL, and (iii) increased thermionic carrier escape rates from the QWs. Increasing the temperature above 400 K causes a reduction in the spectral response at all biased conditions. Increasing bias tends to increase the spectral responsivity of the MQW structure. An increase in the bias voltage causes more QWs to fall in the SCR leading to a higher spectral response [21]. The peak spectral responsivity of the sample showed a slight decrease from 100 to 300 K at -2 V bias. This trend was observed again at -4 V and -6 V bias from 100 to 200 K. It is also observed that the photocurrent tends to saturate at higher biased conditions, i.e., the change in spectral responsivity from zero bias to -2 V bias is more prominent as compared to the change from -4 V to -6 V bias.

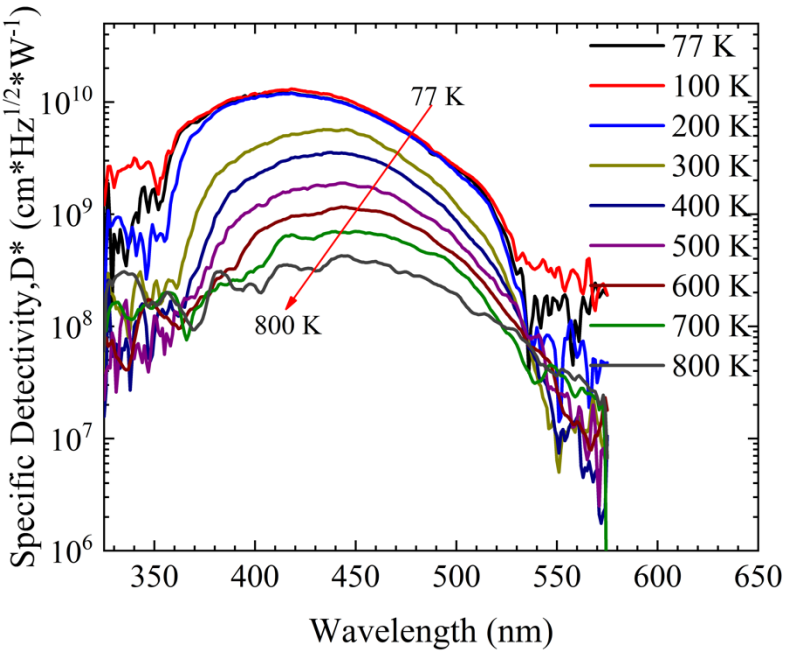

Figure 5.6. The specific detectivity, D*, of the InGaN/GaN MQW structure plotted as a function of wavelength for different temperatures at zero bias.

The specific detectivity of the MQW structure is extracted using the 1Hz equivalent noise bandwidth of the measurement setup at zero bias and shown in Fig. 5.6 for different temperatures. The detectivity of the device is prominent at a wavelength range corresponding to the barrier heights. A drop in the detectivity is observed when the temperature increases from 77 to 800 K. A high noise current due to thermally generated carriers at high temperature causes the reduction in

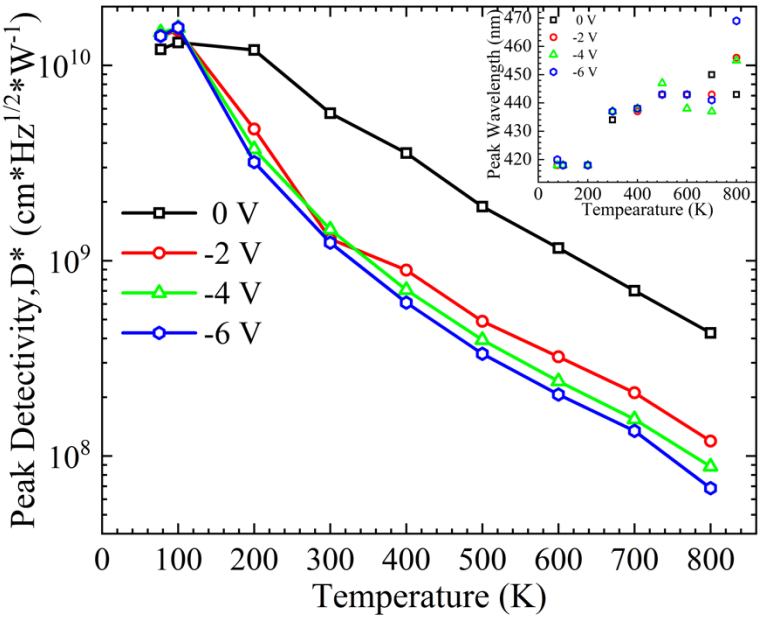

Figure 5.7. The peak specific detectivity of the InGaN/GaN MQW structure as a function of temperature at different biased conditions. Inset shows the evolution of wavelength corresponding to the peak specific detectivity.

the detectivity at elevated temperatures. It is found that a peak detectivity of 4 x 108 cmHz$^{1/2}$W^{-1} is achievable at 800 K with zero bias at 440 nm. Figure 5.7 shows the evolution of peak detectivity of the MWQ structure with temperature for different biased conditions; inset shows the evolution of wavelength corresponding to the peak specific detectivity. The sample shows the highest detectivity at zero biased conditions at temperatures above 100 K. The noise performance of the MQW structure is superior at zero bias conditions. The degradation of the noise performance is

only two-order of magnitude over the temperature range of 77 – 800 K at zero bias compared to a three-order magnitude degradation at all other biases. A high detectivity at zero biased condition indicates a high rate of change of noise than that of responsivity when the applied bias increases. This behavior suggests that the detectivity of the MQW structure is limited to the bias-induced internal noise.

5.5. Conclusion

The high-temperature behavior of the InGaN/GaN MQW photodiode structure is studied up to 800 K. The noise analysis on the device is conducted using a 1 Hz equivalent noise bandwidth of the measurement setup at photovoltaic and biased modes for a wide range of temperatures. The spectral response shows an increase in the response up to 400 K and degrades at higher temperatures. The spectral responsivity of the sample increases with the increase in the bias. However, the specific detectivity degrades with applied bias voltages due to the higher bias-induced internal noise. The sample shows a two-order of magnitude reduction in the specific detectivity at photovoltaic mode compared to a three-order of magnitude reduction at biased modes. The MQW structure shows a peak detectivity of 4 x 108 $cmHz^{1/2}W^{-1}$ at 800 K with zero bias at 440 nm.

References

[1] W. Shockley, “Silicon Carbide - a High Temperature Semiconductor,” Proceedings of Oxford Symposium Publications Division, Pergamon Press, 1960.

[2] N. Kaminski, "State of the art and the future of wide band-gap devices," 13th European Conference on Power Electronics and Applications, Barcelona, pp. 1-9, 2009.

[3] M. Kanechika, T. Uesugi, and T. Kachi, “Advanced SiC and GaN power electronics for automotive systems,” 2010 International Electron Devices Meeting, 2010.

[4] H. A. Mantooth, M. D. Glover, and P. Shepherd, “Wide Bandgap Technologies and Their Implications on Miniaturizing Power Electronic Systems,” IEEE Journal of Emerging and Selected Topics in Power Electronics, vol. 2, no. 3, pp. 374–385, 2014.

[5] N. Ericson, S. Frank, C. Britton, L. Marlino, S.-H. Ryu, D. Grider, A. Mantooth, M. Francis, R. Lamichhane, M. Mudholkar, P. Shepherd, M. Glover, J. Valle-Mayorga, T. Mcnutt, A. Barkley, B. Whitaker, Z. Cole, B. Passmore, and A. Lostetter, “A 4H Silicon Carbide Gate Buffer for Integrated Power Systems,” IEEE Transactions on Power Electronics, vol. 29, no. 2, pp. 539–542, 2014.

[6] M. Barlow, A. M. Francis, N. Chiolino, J. Holmes, A. Abbasi, and H. A. Mantooth, “SiC-CMOS digital circuits for high temperature power conversion,” 2016 IEEE 4th Workshop on Wide Bandgap Power Devices and Applications (WiPDA), 2016.

[7] A. Sabbar, S. Madhusoodhanan, S. Al-Kabi, B. Dong, J. Wang, S. Atcitty, R. Kaplar, D. Ding, A. Mantooth, S.-Q. Yu, and Z. Chen, “Systematic Investigation of Spontaneous Emission Quantum Efficiency Drop up to 800K for Future Power Electronics Applications,” IEEE Journal of Emerging and Selected Topics in Power Electronics, pp. 1–1, 2018.

[8] S. Madhusoodhanan, A. Sabbar, S. Atcitty, R. Kaplar, A. Mantooth, S.-Q. Yu, and Z. Chen, “High-Temperature Analysis of GaN-based Blue LEDs for Future Power Electronic Applications,” IEEE Journal of Emerging and Selected Topics in Power Electronics, pp. 1–1, 2019.

[9] A. Sabbar, S. Madhusoodhanan, S. Al-Kabi, B. Dong, J. Wang, S. Atcitty, R. Kaplar, D. Ding, A. Mantooth, S.-Q. Yu, and Z. Chen, “High Temperature and Power Dependent Photoluminescence Analysis on Commercial Lighting and Display LED Materials for Future Power Electronic Modules,” Scientific Reports, vol. 9, no. 1, 2019.

[10] H. Matsunami, “Technological Breakthroughs in Growth Control of Silicon Carbide for High Power Electronic Devices,” Japanese Journal of Applied Physics, vol. 43, no. 10, pp. 6835–6847, Aug. 2004.

[11] E. V. Kalinina, A. M. Ivanov, and N. B. Strokan, “Performance of p-n 4H-SiC film nuclear radiation detectors for operation at elevated temperatures (375 °C),” Technical Physics Letters, vol. 34, no. 3, pp. 210–212, 2008.

[12] A. M. Ivanov, A. V. Sadokhin, N. B. Strokan, and A. A. Lebedev, “On the problem of the radiation hardness of SiC nuclear radiation detectors at high working temperatures,” Semiconductors, vol. 45, no. 10, pp. 1369–1373, 2011.

[13] G. Lioliou, M. Mazzillo, A. Sciuto, and A. Barnett, “Electrical and ultraviolet characterization of 4H-SiC Schottky photodiodes,” Optics Express, vol. 23, no. 17, p. 21657, Nov. 2015.

[14] X. Chen, H. Zhu, J. Cai, and Z. Wu, “High-performance 4H-SiC-based ultraviolet p-i-n photodetector,” Journal of Applied Physics, vol. 102, no. 2, p. 024505, 2007.

[15] A. Kociubi´nski, M. Duk, K. Muzyka, and M. Borecki, “Ultraviolet photodetectors fabricated on 4H-SiC,” in Proceedings of 8th International Conference on Sensor Device Technologies and Applications, pp. 78–80, 2017.

[16] E. Monroy, F. Omn S, and F. Calle, “Wide-bandgap semiconductor ultraviolet photodetectors,” Semiconductor Science and Technology, vol. 18, no. 4, Apr. 2003.

[17] T. D. Veal, P. H. Jefferson, L. F. J. Piper, C. F. Mcconville, T. B. Joyce, P. R. Chalker, L. Considine, H. Lu, and W. J. Schaff, “Transition from electron accumulation to depletion at InGaN surfaces,” Applied Physics Letters, vol. 89, no. 20, p. 202110, 2006.

[18] R. Singh, D. Doppalapudi, T. D. Moustakas, and L. T. Romano, “Phase separation in InGaN thick films and formation of InGaN/GaN double heterostructures in the entire alloy composition,” Applied Physics Letters, vol. 70, no. 9, pp. 1089–1091, Mar. 1997.

[19] R. W. Martin, P. G. Middleton, K. P. O’Donnell, and W. V. D. Stricht, “Exciton localization and the Stokes’ shift in InGaN epilayers,” Applied Physics Letters, vol. 74, no. 2, pp. 263–265, Nov. 1999.

[20] C. Rivera, J. L. Pau, and E. Muñoz, “Photocurrent gain mechanism in Schottky barrier photodiodes with negative average electric field,” Applied Physics Letters, vol. 89, no. 26, p. 263505, 2006.

[21] C. Rivera, J. Pau, A. Navarro, and E. Munoz, “Photoresponse of (In,Ga)N–GaN Multiple-Quantum-Well Structures in the Visible and UVA Ranges,” IEEE Journal of Quantum Electronics, vol. 42, no. 1, pp. 51–58, 2006.

6. High-Temperature Analysis of Optical Coupling Using AlGaAs LEDs for High-Density Integrated Power Modules

6.1. Abstract

A low temperature co-fired ceramic (LTCC)-based optocoupler design is demonstrated as a possible solution for optical isolation in high-density integrated power modules. The design and fabrication of LTCC based package are discussed. AlGaAs double heterostructure is used both as emitter and photodetector in the proposed optocoupler. A detailed study on the electroluminescence and internal quantum efficiency of the AlGaAs structure is conducted. The photosensitivity of the discrete devices is studied using spectral and noise analysis at elevated temperatures. The material figure of merit parameter, D*, is calculated in the temperature range 77 - 800 K. The proposed optocoupler is tested at elevated temperatures, and the results are presented.

6.2. Introduction

Third-generation semiconductor materials such as silicon carbide (SiC) and gallium nitride (GaN) improved the operation in terms of power capability, temperature tolerance, and switching frequencies in the field of power electronics [1-3]. While GaN devices are mainly preferred for applications below 500 V, SiC is the ideal material of choice for power modules with higher voltage and current ratings. Commercially available SiC devices, rated 900 V and above, with a chip size spanning tens of millimeters, enables the development of high-density power modules with a low form factor [4]. A low form factor power electronic system design is vital in size and/or weight-sensitive applications such as aeronautics, hybrid motor drives, and space exploration [5-7]. The miniaturization of the wide bandgap-based power electronic system is mainly made

possible by utilizing the higher junction temperature operations of SiC devices, thus eliminating a bulky cooling system [8,9]. Integrating the gate driver and protection circuity to the power module further reduces the form factor of the system [10-13]. In this integrated power module, the low-voltage passive components of the gate driver and the protection circuitry are placed close to the power devices, making them exposed to similar environmental conditions as the power devices. The volumetric reduction of the integrated power modules is now limited by the passive components in the gate driver circuitry.

To fully utilize the volumetric improvements ensured by the use of SiC technology in the power electronics system, the focus should be on improving the thermal capability of the packaging and the passive components in the design. Most of the passive components, such as resistors, capacitors, and magnetics are rated up to a maximum temperature of 200oC [14]. Spyker et al. reported magnetic material capable of 300oC operation [15]. However, the magnetics, such as isolation transformers, are comparatively bulky in design. The design of a low form factor integrated power modules with bulky isolation transformers is complicated. With the development of a suitable optical isolation system, i.e., optocouplers, volumetric issues associated with the magnetic isolation system can be avoided while simplifying the gate circuitry as well.

In this chapter, we report the high-temperature operation of double heterojunction (DH) aluminum gallium arsenide (AlGaAs) light-emitting diodes (LEDs) as emitter as well as a photodetector. We also report the optical coupling efficiency of these devices when integrated into an LTCC package. The rationale for selecting the AlGaAs structure can be explained by i) overlapping emission and absorption spectra of AlGaAs LEDs at room temperature ii) superior temperature stability and spectral response of GaAs devices over traditional Si devices [16]. The LTCC package was selected due to its higher temperature stability and the ease of integrating into

power module designs [17,18]. Temperature-dependent electroluminescence and spectral response measurements were carried out on bare die devices. The internal quantum efficiency (IQE) of the device is extracted as a function of injected current density for different temperatures. The specific detectivity of the device was calculated from the spectral response measurements. The output current as a function of the input current of the LTCC-based optocoupler is measured and analyzed at elevated temperatures. This study demonstrates the development of high-temperature optocouplers and suggests the possibility of further miniaturization of high-density power modules by eliminating the volumetric issues in design architecture.

6.3. Experiment

AlGaAs DH infrared LEDs with overlapping emission and absorption spectrum at room temperature is selected for high-temperature optical and electrical studies. Bare-die devices are selected to avoid unwanted failures at elevated temperatures due to the degradation of packaging media or forming lenses on the chip surface. High-temperature characterization of the LEDs was carried out in a Janis ST-100 cryostat. A Horiba 550 spectrometer integrated with a photomultiplier tube (PMT) is used for temperature- and intensity-dependent electroluminescence (T-IDEL) measurements [19]. The spectral responses of the structure were obtained using a tunable monochromator with a 250W, 24V tungsten halogen lamp. The incident power on the LEDs is measured using a calibrated silicon detector. A lock-in amplifier is used to measure the photocurrents. The dark current-voltage (I-V) characteristics in the temperature range 77 - 800 K is measured using a Keithley 236 source measurement unit (SMU). The bare die devices were integrated into an LTCC-based optocoupler package for high-temperature measurements. The high-temperature measurements were performed in a Janis ST-100 cryostat.

6.4. LTCC Packaging

The LTCC package is fabricated at the University of Arkansas (UA) High-Density Electronic Center (HiDEC) facility. The detailed fabrication process is shown in Fig. 6.1. LTCC fabrication mainly has six steps.

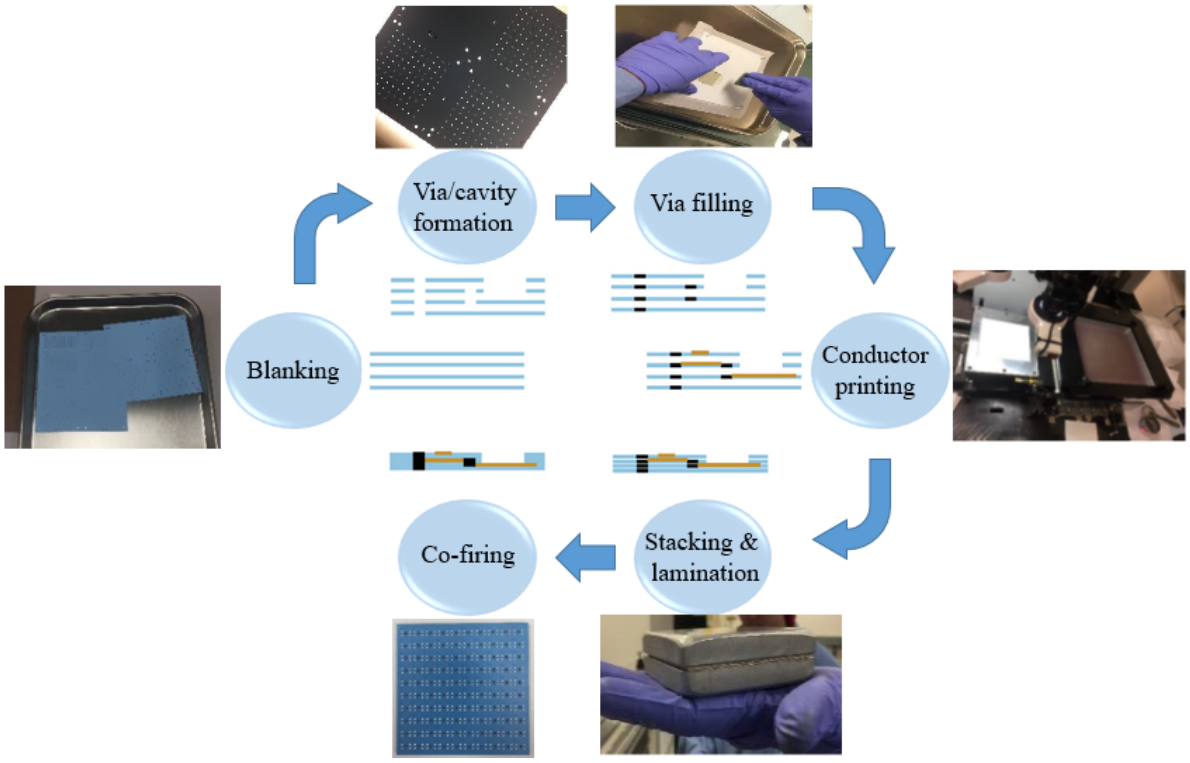

Figure 6.1 The fabrication process flow of high temperature optocoupler packaging.

(a) Blanking & Pre-conditioning: The LTCC tape is blanked at the process coupon size and pre-conditioned in a convection oven.

(b) Via hole / Cavity forming: Registration and via holes are mechanically punched.

(c) Via filling: Via holes are filled using a porous film print nest by pressing via fill paste through the holes using a squeegee.

(d) Conductor/passives printing: Conductors and passives are deposited using screen printing techniques.

The previous steps are carried out for every layer of the circuit. Sheets are inspected after each step. The following steps are carried out for each fabricated coupon:

(e) Stacking & lamination: Layers are stacked and tacked using the registration holes created at the beginning of the process. The stack-up is laminated using an isostatic press in order to guarantee maximum process repeatability and avoid de-lamination.

(f) Co-Firing: The laminated coupon is finally fired in a sintering oven.

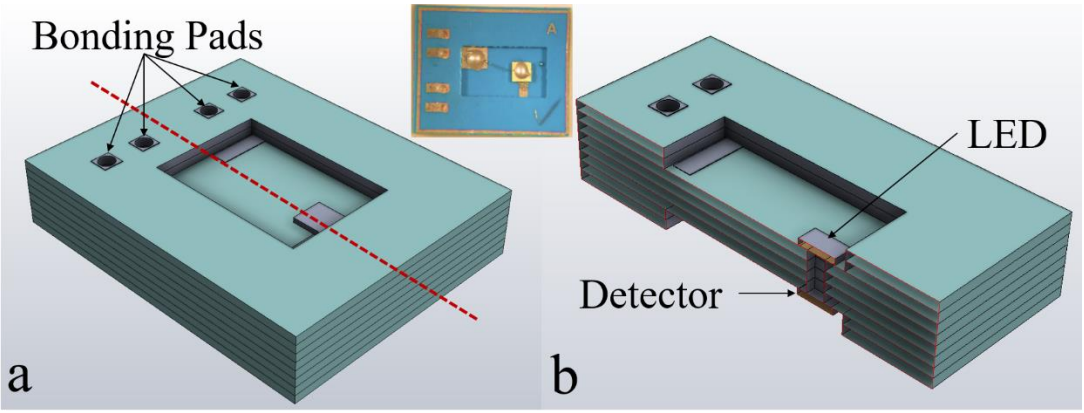

Figure 6.2. a) 3D CAD design of the LTCC based optocoupler, b) cross sectional view. Inset shows the fabricated device.

Figure 6.2 shows the 3D design of the LTCC package; inset shows the fabricated device. The package is made of eight layers of DuPont GreenTape 951 with a thickness of 254 um. The separation between LED and detector is around 1 mm. After firing, the total volume of the package is around 10*8*1.7 mm3.

6.5. Results and Discussion

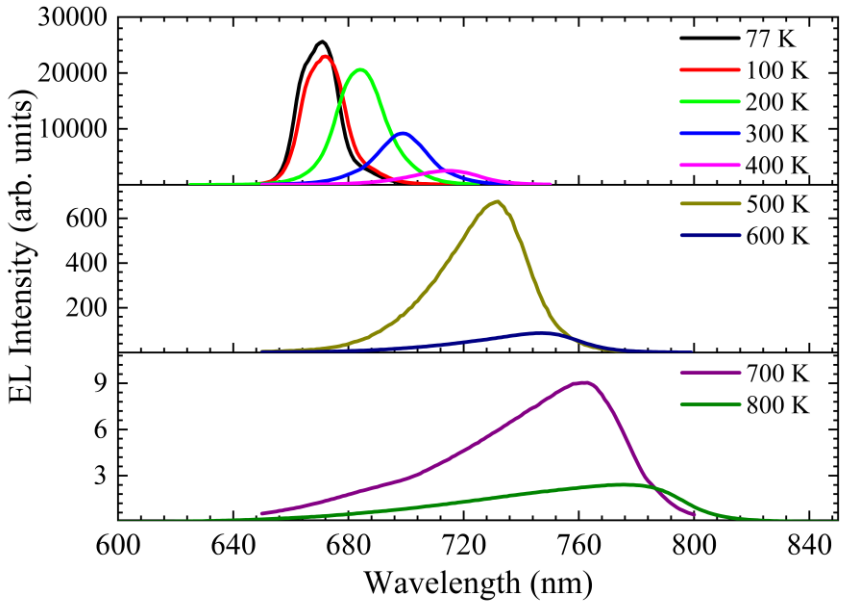

Figure 6.3. The EL spectra of the AlGaAs DH is measured at a current density of 0.325A/cm2 for different temperatures.

The evolution of the EL spectra of the AlGaAs DH structure over the temperature is shown in Fig.6.3 with an injected current density of 0.325 A/cm2. A decrease in the EL intensity, as well as a spectrum broadening, is observed at higher temperatures. The spectral peak of the DH structure exhibits redshift at elevated temperatures from 670 nm at 77 K to 784 nm at 800 K. The shift of the spectral peak is attributed to the bandgap narrowing effect at elevated temperatures [20]. Significant reduction in the EL intensity is observed when the temperature is increased from 77 K to 800 K. A four orders of magnitude reduction in the EL intensity at elevated temperatures indicates a severe drop in IQE. However, the temperature droop, i.e., the reduction in IQE due to high temperatures, is also dependent on the injected current density. A detailed understanding of

the IQE behavior w.r.t the injected current density enables the optimal selection of biasing conditions for LEDs to achieve a minimal drop in IQE at elevated temperatures.

To further study the behavior of AlGaAs LEDs at higher temperatures, IQE of the LEDs were extracted using the ABC model. Figure 6.4 shows IQE as a function of injected current density for different temperatures. The dots are the experimental points, and the solid lines are extracted using the ABC model. The efficiency drop at higher injected current densities, often called current droop, leads to the dome-like structure of the IQE curves. The current droop behavior is due to the enhanced Auger recombination mechanism, a non-radiative recombination

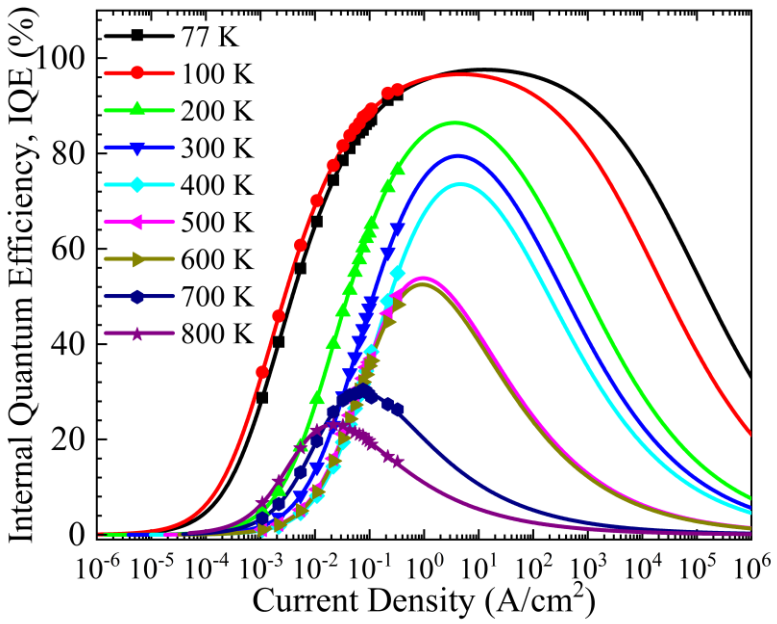

Figure 6.4. Internal quantum efficiency is plotted as a function of current density at different temperatures.

mechanism, which suppresses the radiative recombination at higher injected current densities [21]. It is observed that at higher temperatures, auger recombination starts to dominates over radiational recombination at relatively lower injected current densities leading to the peak IQE occurs at lower injected current densities. The LED shows a peak quantum efficiency of 97.58 % at 77 K. The

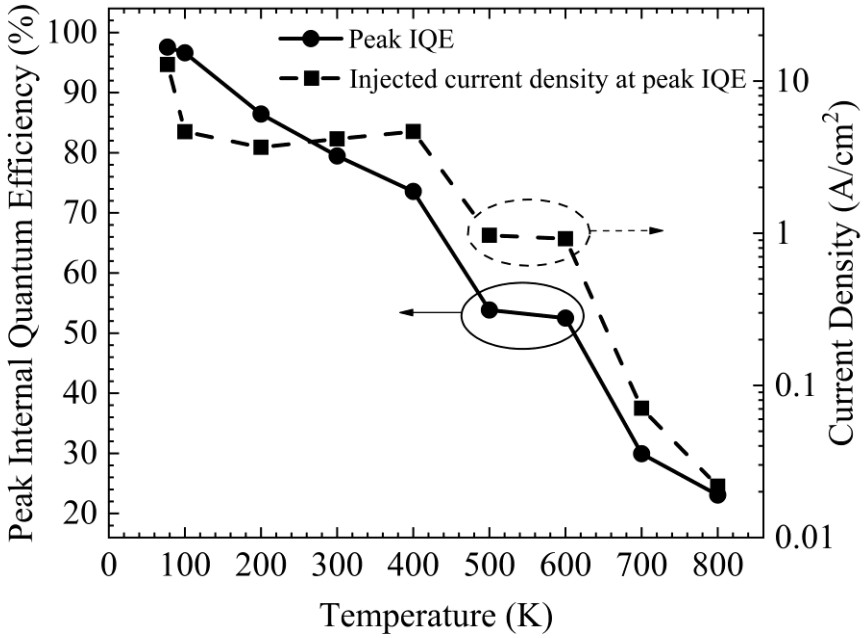

Figure 6.5. The peak IQE and the corresponding injected current density are extracted and plotted as a function of temperatures.

peak IQE of the device decreases with an increase in temperature. At 800 K, the device exhibits a peak IQE of 23.08 %. The extracted values of the PIQE and corresponding injected current densities (jPIQE) are plotted as a function of temperature, as shown in Fig.6.5. The device exhibits a linear drop in IQE from 77 K to 400 K, with approximately a reduction of 7 % IQE in every 100 K. Increasing the temperature beyond 400 K shows a severe reduction in IQE from 73.57 % at 400

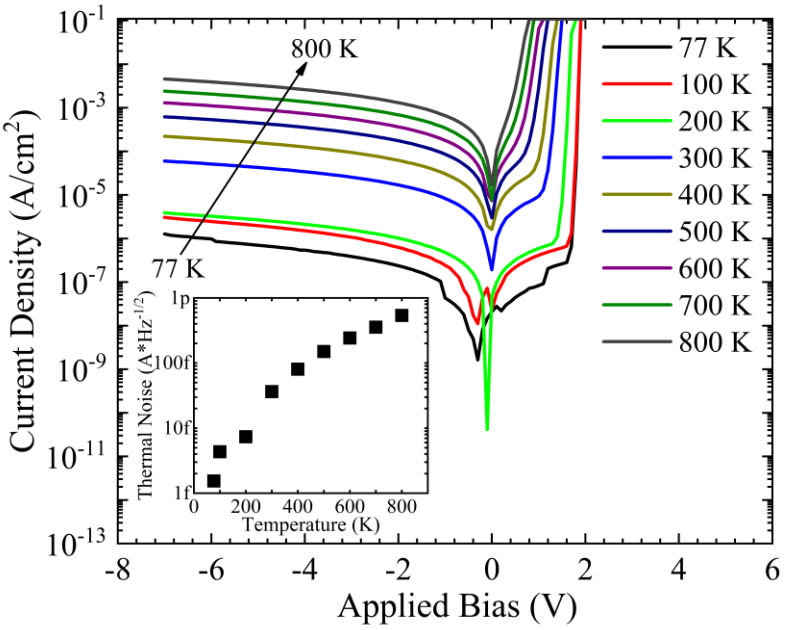

Figure 6.6. I-V characteristics of the ALGaAs DH for temperatures from 77 - 800 K. Inset shows the evolution of thermal noise.

K to 53.83 % at 500 K. The peak current respective to the peak IQE follows a similar trend that of PIQE with an increase in temperature. The jPIQE reduced from 12.85 A/cm2 at 77 K to 21.77 mA/cm2 at 800 K. Low jPIQE enables the device to work at peak IQE with minimal self-heating.

Stable operation at 800 K and an overlapping emission and absorption spectra lead to a detailed study on the photodetection characteristics of the AlGaAs DH structure. Figure 6.6 shows the dark IV characteristics of the structure from 77 - 800 K, the inset shows the evolution of thermal noise with temperature. An exponential rise in thermal noise is observed from the structure at elevated temperatures. Three orders of magnitude change in the leakage current is observed when the temperature is increased from 77 K to 800 K. A sudden increase in the leakage current as well as the thermal noise at 300 K is attributed to the thermal ionization of carriers from deep traps and trap assisted tunneling process [22]. The spectral response of the device at zero biased condition

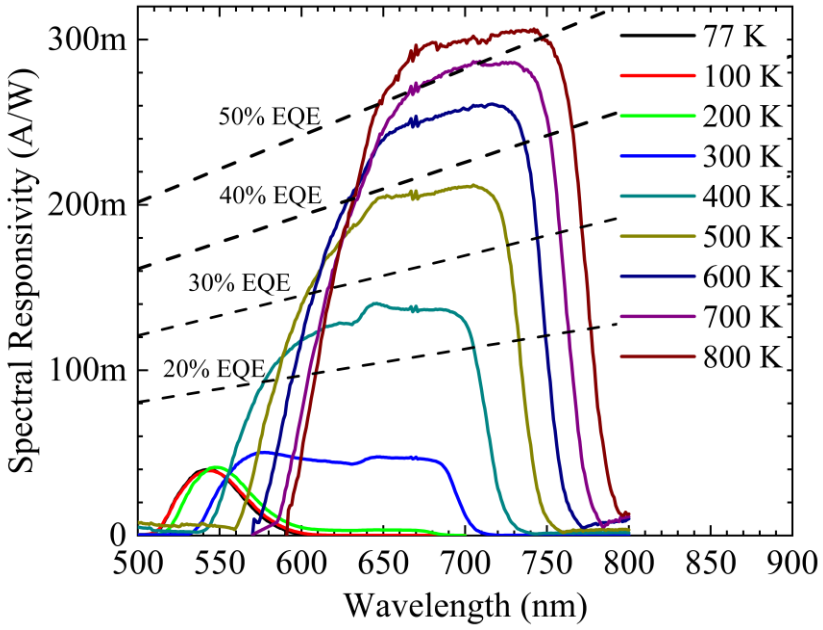

Figure 6.7. Spectral response of the structure for different temperatures at zero bias. Dashed lines represent the spectral response to achieve marked EQE.

is shown in Fig. 6.7 for different temperatures; the dashed line represents spectral responsivity with a specified external quantum efficiency (EQE) across the measured wavelength. An enhanced spectral response is observed at elevated temperatures. The spectral response curves exhibit a large redshift in the spectral response peak and the detection edge at elevated temperatures. An increase in temperature shifts the absorption spectrum of the structure to longer wavelengths by reducing the effective bandgap.

The evolution of the peak spectral responsivity of the structure with temperature for different biased conditions is shown in Fig.6.8; inset shows the respective wavelength at which the spectral peak is observed. The structure shows a relatively small increment in the spectral peak at lower temperatures. Increasing the temperature above 300 K results in an exponential change in the responsivity. The rapid increase in the spectral responsivity above 300 K is attributed to i) shift

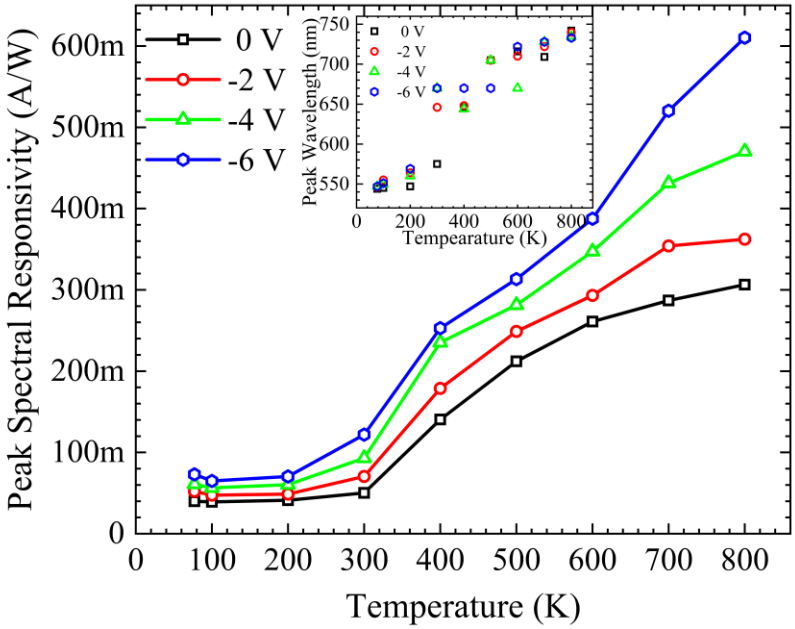

Figure 6.8. Peak spectral response of the AlGaAs DH is plotted as a function of temperature for different biased conditions. Inset shows the evolution of wavelength corresponding to the peak spectral response.

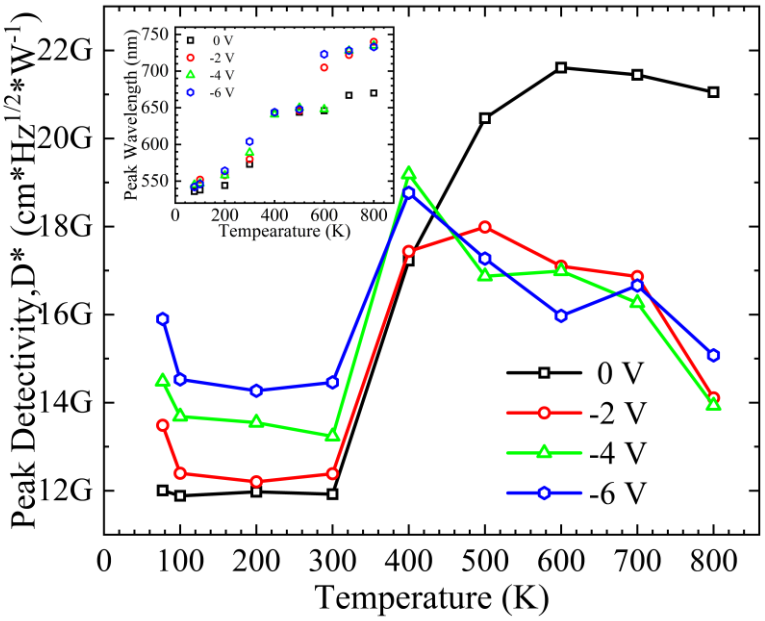

Figure 6.9. The peak specific detectivity as a function of temperature at different biased conditions. Inset shows the evolution of wavelength corresponding to the peak specific detectivity.

in the absorption spectrum towards higher wavelengths due to bandgap shrinkage, as shown in the

inset of Fig. 6.8 ii) reduced absorption rate at higher wavelength leads to more photons reaching the active area resulting in a higher responsivity. Biasing the structure with higher voltages leads to a wider space charge region resulting in enhanced spectral responsivity, as shown in Fig. 7. At elevated temperatures, the spectral peak responsivity tends to saturate at 800 K for lower bias curves. However, no sign of saturation in the spectral peak response is visible for higher biased curves, even at 800 K.

The specific detectivity, D*, of the structure is extracted for different temperatures and biased conditions to quantify the performance of the photosensitivity of the structure. Figure 6.9 shows the peak specific detectivity as a function of temperature for different biased conditions; inset shows the wavelength at which peak detectivity is observed. The structure exhibits slight variation in the D* at lower temperatures. At zero bias, the D* of the structure increased from 12G Jones (cmHz1/2W-1) at 300 K to 17G Jones at 400 K. A rapid increase in the D* at 400 K is attributed to the increase in the spectral responsivity due to a significant redshift with minimal increase in the leakage current and thermal noise. The structure showed a peak D* of 22G Jones at zero bias when the temperature increased to 600 K. At zero bias condition, the D* starts to decline at temperatures above 600 K. However, at biased conditions, the D* starts to decline at temperatures above 400 K. It is also observed that applying a bias voltage leads to a decline in D* of the structure at temperatures above 400 K. Although the structure shows a linear increase in spectral responsivity with bias voltage at elevated temperatures, higher noise current at biased conditions leads to a reduced D*. At elevated temperatures, the photosensitive performance of the structure is limited by bias-induced internal noise. A superior noise performance at zero bias at

elevated temperatures indicates that a high rate of change of noise than that of responsivity when the applied bias increases.

High-temperature analysis of the emitter and photodetector operation of the discrete

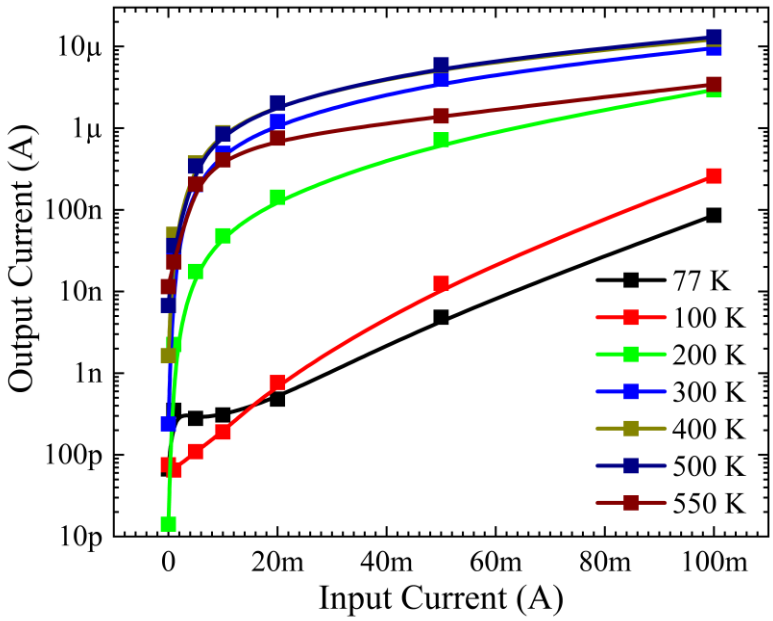

Figure 6.10. The output current of the fabricated LTCC based optocoupler is plotted as a function of the input current for different temperatures.

devices is followed by the design and fabrication of the LTCC package. The individually tested devices are integrated into the LTCC package, thus creating an optocoupler, and tested the optical coupling efficiency at elevated temperatures. The output current of the integrated LTCC based optocoupler is shown in Fig. 6.10 without any external amplification. The input current to the LED is varied from 0 to 100 mA, and the detector is biased at zero voltage. The device shows comparatively low current transfer ratio (CTR) values below 300 K. A lower CTR values at temperatures below 300 K is attributed to the reduced spectral response of the AlGaAs DH structure. Although the LED performance degrades with an increase in temperature, the spectral

response of the structures improves at elevated temperature leading to higher CTR values at temperatures above 200 K. The CTR value of the structure starts to degrade at temperatures above 500 K. A reduced CTR value is recorded at 550 K. Temperatures above 550 K, the structure failed to output any photocurrent. The samples were unmounted and confirmed the absence of any failures due to packaging. It is concluded that a higher degradation of the EL intensity at temperatures above 500 K causes the CTR to drop. It is observed that the rate of degradation of the EL intensity is dominating over the enhanced spectral responsivity at higher temperatures. Stable CTR values in the temperature range of 300 to 550 K is promising in the development of high-temperature optocouplers for future high-density integrated power modules.

6.6. Conclusion

A high-temperature optocoupler based on LTCC packaging is demonstrated as a possible solution for optical isolation in future high-density power modules. An LTCC based optocoupler package is fabricated using eight layers of DuPont GreenTape 951 with a thickness of 254 um. After firing, the total volume of the package is around 10*8*1.7 mm3. AlGaAs DH devices are integrated into the LTCC package, both as emitter and photodetector, with a separation of 1mm. Detailed analysis of the high-temperature behavior of AlGaAs DH structure as both emitter and photodetector is conducted over the temperature range from 77 - 800 K. While the EL spectra of the discrete AlGaAs structure reduces with temperature, and enhanced spectral response is observed at elevated temperatures. The LED structure shows a significant red shift in the EL spectra, as well as the detection range from 670 nm at 77 K to 784 nm at 800 K. The LED structure exhibits an IQE of 22 % at 800 K. The photosensitivity of the structure is quantified using the material figure of merit parameter, D*. A peak detectivity of 22G Jones at zero bias is observed at

600 K. The fabricated optocoupler shows a stable operation in the temperature range of 300 – 550 K.

References

[1] W. Shockley, “Silicon Carbide - a High Temperature Semiconductor,” Proceedings of Oxford Symposium Publications Division, Pergamon Press, 1960.

[2] N. Kaminski, "State of the art and the future of wide bandgap devices," 13th European Conference on Power Electronics and Applications, Barcelona, pp. 1-9, 2009.

[3] M. Kanechika, T. Uesugi, and T. Kachi, “Advanced SiC and GaN power electronics for automotive systems,” 2010 International Electron Devices Meeting, 2010.

[4] H. A. Mantooth, M. D. Glover, and P. Shepherd, “Wide Bandgap Technologies and Their Implications on Miniaturizing Power Electronic Systems,” IEEE Journal of Emerging and Selected Topics in Power Electronics, vol. 2, no. 3, pp. 374–385, 2014.

[5] Z. Cole, B. Passmore, B. Whitaker, A. Barkley, T. Mcnutt, and A. Lostetter, “Packaging of High Frequency, High Temperature Silicon Carbide (SiC) Multichip Power Module (MCPM) Bi-directional Battery Chargers for Next Generation Hybrid Electric Vehicles,” International Symposium on Microelectronics, vol. 2012, no. 1, pp. 001105–001115, 2012.

[6] R. Szweda, “Applications market overview,” Gallium Nitride and Related Bandgap Materials and Devices, pp. 33–103, 2000.

[7] G. A. Carr, C. J. Iannello, Y. Chen, D. J. Hunter, L. D. Castillo, A. T. Bradley, C. Stell, and M. M. Mojarradi, “Extreme environment capable, modular and scalable power processing unit for solar electric propulsion,” 2013 IEEE Aerospace Conference, 2013.

[8] P. Neudeck, M. Krasowski, and N. Prokop, “(Invited) Assessment of Durable SiC JFET Technology for 600° to -125° Integrated Circuit Operation,” 2011.

[9] T. Funaki, J. Balda, J. Junghans, A. Kashyap, F. Barlow, A. Mantooth, T. Kimoto, and T. Hikihara, “Power Conversion with SiC Devices at Extremely High Ambient Temperatures,” IEEE 36th Conference on Power Electronics Specialists, 2005.

[10] P. Anthony, N. Mcneill, and D. Holliday, “High-speed resonant gate driver with controlled peak gate voltage for silicon carbide MOSFETs,” 2012 IEEE Energy Conversion Congress and Exposition (ECCE), 2012.

[11] Y. Zushi, S. Sato, K. Matsui, Y. Murakami, and S. Tanimoto, “A novel gate assist circuit for quick and stable driving of SiC-JFETs in a 3-phase inverter,” 2012 Twenty-Seventh Annual IEEE Applied Power Electronics Conference and Exposition (APEC), 2012.

[12] J.-S. Chen, S.-H. Ryu, and K. Kornegay, “A silicon carbide CMOS intelligent gate driver circuit,” Conference Record of 1998 IEEE Industry Applications Conference. Thirty-Third IAS Annual Meeting (Cat. No.98CH36242).

[13] A. Lostetter, J. Hornberger, B. Mcpherson, B. Reese, R. Shaw, M. Schupbach, B. Rowden, A. Mantooth, J. Balda, T. Otsuka, K. Okumura, and M. Miura, “High-temperature silicon carbide and silicon on insulator based integrated power modules,” 2009 IEEE Vehicle Power and Propulsion Conference, 2009.

[14] R. Wang, P. Ning, D. Boroyevich, M. Danilovic, F. Wang, and R. Kaushik, “Design of high-temperature SiC three-phase AC-DC converter for >100°C ambient temperature,” 2010 IEEE Energy Conversion Congress and Exposition, 2010.

[15] R. Spyker, J. Huth, I. Mehdi, and A. Brockschmidt, “300C ferrite material for high temperature magnetics,” 2004 IEEE 35th Annual Power Electronics Specialists Conference (IEEE Cat. No.04CH37551).

[16] I. Amiri, F. M. A. M. Houssien, A. N. Z. Rashed, and A. E.-N. A. Mohammed, “Temperature effects on characteristics and performance of near-infrared wide bandwidth for different avalanche photodiodes structures,” Results in Physics, vol. 14, p. 102399, 2019.

[17] A. Pietrikova, T. Girasek, P. Lukacs, T. Welker, and J. Müller, “Simulation of cooling efficiency via miniaturised channels in multilayer LTCC for power electronics,” Journal of Electrical Engineering, vol. 68, no. 2, pp. 132–137, 2017.

[18] B. Banijamali, S. Ramalingam, N. Kim, and C. Wyland, “Ceramics vs. low-CTE organic packaging of TSV silicon interposers,” 2011 IEEE 61st Electronic Components and Technology Conference (ECTC), 2011.

[19] S. Madhusoodhanan, A. Sabbar, S. Atcitty, R. Kaplar, A. Mantooth, S.-Q. Yu, and Z. Chen, “High-Temperature Analysis of GaN-based Blue LEDs for Future Power Electronic Applications,” IEEE Journal of Emerging and Selected Topics in Power Electronics, pp. 1–1, 2019.

[20] Y. Varshni, “Temperature dependence of the energy gap in semiconductors,” Physica, vol. 34, no. 1, pp. 149–154, 1967.

[21] E. Yablonovitch and E. Kane, “Reduction of lasing threshold current density by the lowering of valence band effective mass,” Journal of Lightwave Technology, vol. 4, no. 5, pp. 504–506, 1986.

[22] Neumark, Gertrude F.; Kuskovsky, Igor L, Wide Bandgap Light Emitting Materials and Devices. Wiley, 2007.

7. Conclusions and Future Work

A high-temperature optocoupler is designed and fabricated to replace isolation transforms as the galvanic isolation solution for the 3D integration of high-density power modules. The proposed optocoupler delivers a continuous operation at 250oC with a lifetime of 10 years. Optical and electrical studies were conducted on gallium nitride (GaN), and silicon carbide (SiC) based optoelectronics materials and devices at elevated temperatures (~550oC). Low temperature co-fired ceramic (LTCC) based optocoupler packaging is designed and fabricated to accommodate LEDs and photodetectors. The discrete optocouplers fabricated from LTCC may integrated to the gate driver circuitry of the high-density power module and tested at elevated temperatures.

7.1. High-Temperature Optical Device Characterization

7.1.1. Commercial Gallium-Nitride-Based Blue LEDs

LEDs primarily fabricated for lighting applications are evaluated at high temperatures (up to 700 K – All temperature units will be in Kelvin from here onwards) for possible integration as an optocoupler emitter in high-density power electronic modules. The temperature- and injection-current-dependent internal quantum efficiency and current-voltage characteristics of the blue LEDs are studied. The IQE has extracted from the measured EL intensity at different temperatures using the ABC model. As per the ABC model, the LED can operate at 700 K with an IQE of 58.50% when it operates at a current density of 2A/cm2. The results show that for a temperature range of 77 – 700 K, the minimum deviation of IQE occurs when the injected current density is between 1 to 10 A/cm2. Normalized external quantum efficiency (EQE) of the device at different temperatures were also extracted using the ABC model.

7.1.2. InGaN/GaN MQW LEDs

High-temperature optical analysis of three different InGaN/GaN MQW LED structures (peak wavelength λp = 448nm, 467 nm & 515nm) is conducted for possible integration as an optocoupler emitter in high-density power electronic modules. The commercially available LEDs, primarily used in the display (λp = 467 nm & 515nm) and lighting (λp = 448nm) applications, are studied and compared to evaluate if they can satisfy the light output requirements in the optocouplers at high temperatures. The temperature- and intensity-dependent electroluminescence measurement technique is used to study the IQE of the LEDs. All three LEDs exhibits above 70 % IQE at 500 K, and stable operation at 800 K without flickering or failure. At 800K, a promising IQE of above 40 % is observed for blue for display (λp = 467 nm) and green for display (λp = 515nm) samples. Blue for light (λp = 448nm) sample shows 24 % IQE at 800 K.

7.1.3. MQW Structure as Detectors

The InGaN/GaN MQW structure is demonstrated as a possible solution for high-temperature photodiode applications. High temperature spectral and noise analysis of InGaN/GaN MQW structure are performed for the potential integration as a detector in future power electronics applications. The spectral response was measured under photovoltaic and bias modes for the temperature range of 77 - 800 K. Figure 8 shows the calculated spectral responsivity of the sample at zero bias voltage. A peak spectral responsivity of 27.0 mA/W at 440 nm at 500 K is recorded. The peak external quantum efficiency of the device was calculated to be in the range of 5 - 8 % in the temperature range 77 - 800 K. The photodetector sensitivity of the structure is quantified using the material figure of merit parameter, D* for different temperature and biased voltages. The specific detectivity of the MQW structure is extracted using the 1Hz equivalent noise bandwidth

of the measurement setup at zero bias and shown in Fig. 9 for different temperatures. A peak detectivity of 4 x 108 cmHz1/2W-1 is observed at 800 K with zero bias at 440 nm.

7.2. High-Temperature Optical Packaging

A study conducted on the packaging options for the high-temperature optocouplers by investigating commercially available packaging architectures. A thorough investigation of the commercially available optocoupler packaging structure was conducted. The main factors to focus on were the packaging material, spacing between the discrete devices, dielectric material used in the packaging, and the orientation of discrete devices. The possible packaging design suitable for high-temperature optocouplers were also investigated. Based on the study, the initial packaging prototype based on LTCC is created. The fabrication of the novel high-temperature packaging prototype on LTCC and initial testing were completed.

7.3. High-Temperature Optocoupling

A high-temperature optocoupler based on LTCC packaging is demonstrated as a possible solution for optical isolation in future high-density power modules. An LTCC based optocoupler package is fabricated using eight layers of DuPont GreenTape 951 with a thickness of 254 um. After firing, the total volume of the package is around 10*8*1.7 mm3. AlGaAs double heterostructure devices are integrated into the LTCC package, both as emitter and photodetector, with a separation of 1mm. Detailed analysis of the high-temperature behavior of AlGaAs DH structure as both emitter and photodetector is conducted over the temperature range from 77 - 800 K. While the EL spectra of the discrete AlGaAs structure reduces with temperature, and enhanced spectral response is observed at elevated temperatures. The LED structure shows a significant red shift in the EL spectra, as well as the detection range from 670 nm at 77 K to 784 nm at 800 K.

The LED structure exhibits an IQE of 22 % at 800 K. The photosensitivity of the structure is quantified using the material figure of merit parameter, D*. A peak detectivity of 22G Jones at zero bias is observed at 600 K. The fabricated optocoupler shows a stable operation in the temperature range of 300 – 550 K.

7.4. Future Work

7.4.1. On-chip Optocoupling

A highly scaled Optocoupling can be achieved by on-chip galvanic isolation, a monolithically integrated optocoupler. In silicon CMOS technology, the photon emitter and detector have to be realized with silicon, an indirect bandgap material, which generally considered as unsuitable for photon emission. One of the main challenges in integrating silicon LEDs and detector in standard CMOS to achieve optocoupling is to overcome the poor overlap between the emission and responsivity spectrum of silicon diodes. However, early studies have suggested that better overlap can be achieved by operating silicon LED in avalanche mode, but with very low efficiency. When in avalanche mode, highly energetic electrons, hot electrons, can have energies from the low end of the conduction band at 1.1 eV to the high end of the conduction band at 3.5 eV. When these electrons recombine with a hole in the valence band, with the right momentum supplied by the crystal phonons, a photon can be generated with energies from 1.1 to 3.5 eV.

Although a highly scaled Optocoupling is possible with on-chip Si technology, a temperature operation is not viable. High-temperature operation can be achieved by creating an wide bandgap based on-chip optocoupler. The GaN technology would be an ideal candidate for on-chip high temperature Optocoupling. However, for applications in the field of high voltage power electronics, creating a SiC-based on-chip optocoupling is strongly recommended. Silicon carbide photodetectors are widely accepted as a high temperature alternative for Si technology.

Although SiC is a indirect bandgap materials, light emission is from SiC LEDs are demonstrated earlier with lower efficiencies. Therefore, working towards to achieve a SiC-based on-chip optocoupler is highly necessary.

Appendix: All Publications

Conferences

1. **S. Madhusoodhanan**, S. Koukourinkova, T. White, Z. Chen, Y. Zhao and M. E. Ware, "Highly linear temperature sensor using GaN-on-SiC heterojunction diode for Harsh environment applications," 2016 IEEE 4th Workshop on Wide Bandgap Power Devices and Applications (WiPDA), Fayetteville, AR, 2016, pp. 171-175. doi: 10.1109/WiPDA.2016.7799932

2. A.Sabbar*, S. Madhusoodhanan*, S. Al-Kabi, B. Dong, J. Wang, S. Atcitty, R. Kaplar, A. Mantooth, S. Yu, and Z. Chen, "High Temperature Photoluminescence of InGaN-Based MQWs on Patterned Sapphire Substrates," IEEE Photonics Conference (IPC), Reston, VA, 2018

3. **S. Madhusoodhanan***, A. Sabbar,* S. Al-Kabi, S. Atcitty, R. Kaplar, A. Mantooth, S-Q. Yu, and Z. Chen, "Temperature dependent optical characterization of GaN based LEDs for high temperature power electronic modules." 13th International Conference on Nitride Semiconductors 2019 (ICNS-13).

4. A. Sabbar, **S. Madhusoodhanan**, S. Al-Kabi, B. Dong, J. Wang, S. Yu, and Z. Chen, "Investigation of High Temperature Photoluminescence Efficiency from InGaN/GaN MQWs," in Conference on Lasers and Electro-Optics, OSA Technical Digest (online) (Optical Society of America, 2018), paper JTh2A.79.

5. A. Sabbar*, **S. Madhusoodhanan***, S. Al-Kabi, B. Dong, J. Wang, S. Atcitty, R. Kaplar, A. Mantooth, S. Yu, and Z. Chen, "High Temperature Spontaneous Emission Quantum Efficiency Analysis from Blue and Green LED Materials," IEEE Photonics Conference (IPC), San Antonio, TX, 2019

6. A. Sabbar, **S. Madhusoodhanan**, H. Tran, B. Dong, J. Wang, A. Mantooth, S. Yu, and Z. Chen, " Investigation of High Temperature LED and Photodetector from InGaN/GaN MQWs," in Conference on Lasers and Electro-Optics, OSA Technical Digest (online) (Optical Society of America, 2020), paper JTh2A.16.

Journals

1. **S. Madhusoodhanan**, S. Sandoval, Y. Zhao, M. E. Ware and Z. Chen, "A Highly Linear Temperature Sensor Using GaN-on-SiC Heterojunction Diode for High Power Applications," in IEEE Electron Device Letters, vol. 38, no. 8, pp. 1105-1108, Aug. 2017, DOI: https://doi.org/10.1109/LED.2017.2714865
2. **S. Madhusoodhanan**, A. Sabbar, S. Al-Kabi, S. Atcitty, R. Kaplar, B. Dong, J. Wang, S. Yu, Z. Chen "High-Temperature Optical Characterization of Wide Band Gap Light Emitting Diodes and Photodiodes for Future Power Module Application", Advances

in Science, Technology and Engineering Systems Journal, vol. 4, no. 2, pp. 17-22 (2019), DOI: http://dx.doi.org/10.25046/aj040203

3. A. Sabbar*, **S. Madhusoodhanan***, S. Al-Kabi, B. Dong, J. Wang, S. Atcitty, R. Kaplar, D. Ding, A. Mantooth, S. Yu, and Z. Chen, "Systematic Investigation of Spontaneous Emission Quantum Efficiency Drop up to 800K for Future Power Electronics Applications". In production at IEEE Journal of Emerging and Selected Topics in Power Electronics, Nov. 2018, DOI: https://doi.org/10.1109/JESTPE.2018.2882775

4. **S. Madhusoodhanan,** A. Sabbar, S. Atcitty, R. Kaplar, A. Mantooth, S.-Q. Yu, and Z. Chen, "High-Temperature Analysis of GaN-based Blue LEDs for Future Power Electronic Applications," IEEE Journal of Emerging and Selected Topics in Power Electronics, pp. 1–1, 2019, DOI: https://doi.org/10.1109/JESTPE.2019.2945166

5. **S. Madhusoodhanan,** R. Sankaralingam, G. Boselli, and Z. Chen, "Analysis of gate-coupled silicon controlled rectifier on HBM protection under voltage overshoot," Journal of Electrostatics, vol. 102, p. 103394, 2019, DOI: https://doi.org/10.1016/j.elstat.2019.103394

6. A. Sabbar, **S. Madhusoodhanan**, S. Al-Kabi, B. Dong, J. Wang, S. Atcitty, R. Kaplar, D. Ding, A. Mantooth, S.-Q. Yu, and Z. Chen, "High Temperature and Power Dependent Photoluminescence Analysis on Commercial Lighting and Display LED Materials for Future Power Electronic Modules," Scientific Reports, vol. 9, no. 1, 2019, DOI: https://doi.org/10.1038/s41598-019-52126-4

7. **S. Madhusoodhanan**, A. Sabbar, S. Atcitty, R. Kaplar, A. Mantooth, S.-Q. Yu, and Z. Chen, "High-Temperature Optical Characterization of GaN-Based LEDs for Future Power Electronic Modules," physica status solidi (a), 2019, DOI: https://doi.org/10.1002/pssa.201900792

8. **S. Madhusoodhanan**, A. Sabbar, H. Tran, B. Dong, J. Wang, A. Mantooth, S.-Q. Yu, and Z. Chen, "High-Temperature Analysis of GaN-based MQW Photodetector for Optical Galvanic Isolations in High-Density Integrated Power Modules," IEEE Journal of Emerging and Selected Topics in Power Electronics, pp. 1–1, 2020, DOI: https://doi.org/10.1109/JESTPE.2020.2974788

9. A. Sabbar, **S. Madhusoodhanan**, B. Dong, J. Wang, A. Mantooth, S.-Q. Yu, and Z. Chen, "High-Temperature Spontaneous Emission Quantum Efficiency Analysis of Different InGaN MQWs for Future Power Electronics Applications," IEEE Journal of Emerging and Selected Topics in Power Electronics, Accepted.

Patent

1. One provisional patent filed: Zhong Chen, Shui-Qing Yu, Alan Mantooth, Andrea Wallace, Syam Madhusoodhanan, "High Temperature Optoelectronic Devices for Power Electronics"